

Improved PCRLB for radar tracking in clutter with geometry-dependent target measurement uncertainty and application to radar trajectory control

Yifang Shi, *Member, IEEE*, Yu Zhang, Linjiao Fu, Dongliang Peng, Qiang Lu, *Member, IEEE*, Jee Woong Choi and Alfonso Farina, *Life Fellow, IEEE*

This work has been submitted to the IEEE for possible publication. Copyright may be transferred without notice, after which this version may no longer be accessible.

Abstract—In realistic radar tracking, target measurement uncertainty (TMU) in terms of both detection probability and measurement error covariance is significantly affected by the target-to-radar (T2R) geometry. However, existing posterior Cramér-Rao Lower Bounds (PCRLBs) rarely investigate the fundamental impact of T2R geometry on target measurement uncertainty and eventually on mean square error (MSE) of state estimate, inevitably resulting in over-conservative lower bound. To address this issue, this paper firstly derives the generalized model of target measurement error covariance for bistatic radar with moving receiver and transmitter illuminating any type of signal, along with its approximated solution to specify the impact of T2R geometry on error covariance. Based upon formulated TMU model, an improved PCRLB (IPCRLB) fully accounting for both measurement origin uncertainty and geometry-dependent TMU is then re-derived, both detection probability and measurement error covariance are treated as state-dependent parameters when differentiating log-likelihood with respect to target state. Compared to existing PCRLBs that partially or completely ignore the dependence of target measurement uncertainty on T2R geometry, proposed IPCRLB provides a much accurate (less-conservative) lower bound for radar tracking in clutter with geometry-dependent TMU. The new bound is then applied to radar trajectory control to effectively optimize T2R geometry and exhibits least uncertainty of acquired target measurement and more accurate state estimate for bistatic radar tracking in clutter, compared to state-of-the-art trajectory control methods.

Index Terms—T2R geometry, target measurement uncertainty, IPCRLB, radar trajectory control.

I. INTRODUCTION

THE Cramér-Rao Lower Bound (CRLB) is defined as the inverse of Fisher information matrix (FIM) that quantitatively evaluates the maximum information extracted from existing knowledge about the unknown vector [1]. In the context of radar tracking, since the target kinematic state to

be estimated is a random vector and usually time-varying, the posterior CRLB (PCRLB) is then defined and calculated in a Riccati-like recursion manner [2], providing the lowest mean-square error (MSE) bound that any unbiased estimators can achieve in theory. In general, the performance of radar tracking in clutter is dominated by the radar measurement uncertainty that lies on twofold: the measurement origin uncertainty (MOU) due to the presence of clutter and multi-target, and the target measurement uncertainty stemming from random miss-detection and statistical noise corruption. Open literatures are dedicated to extend the preliminary PCRLB in [2] for radar tracking with different levels of radar measurement uncertainties. Such as [3]–[6], [7] introduced the information reduction factor (IRF) into PCRLB to account for the MOU caused by clutter disturbance, [8]–[10] derived the PCRLB for multi-radar tracking problem by further considering the MOU caused by the presence of multitarget, [11] derived the PCRLB for distributed range-only localization with MOU and signal-noise-ratio (SNR)-dependent target detection probability, more recently, [12] derived the exact FIM (EFIM) with the MOU and state-dependent target detection probability, just name a few. However, it is noteworthy that existing literature formulates PCRLB for radar tracking with radar measurement uncertainty under a basic assumption: the target measurement error covariance is independent of the target-to-radar (T2R) geometry. This assumption obviously deviates from the realistic radar operation [12], [13] and inevitably results in over-conservative PCRLBs. Particularly, in bistatic radar system, the TMU in terms of both target detection probability and measurement error covariance are apparently affected by the T2R triangular geometry, which eventually determines the tracking performance [14].

Motivated by the fact that the target measurement uncertainty (TMU) is highly affected by the T2R geometry, along with the fact that radar platform is usually collaborative and capable of maneuvering (e.g., airborne), existing literatures pay tremendous attention to optimize the T2R geometry via controlling the trajectory of radar platform. In such, the radar enables to cognitively adapt its moving path to acquire higher quality target measurement based on perceived environment and eventually improve the tracking performance. The radar trajectory control is essentially a nonlinear control problem that aims to assign radar best state at each sampling time

Yifang Shi, Yu Zhang, Linjiao Fu, Qiang Lu and Dongliang Peng are with the School of Automation, Hangzhou Dianzi University, Hangzhou, 310018, China (e-mail: syf2008@hdu.edu.cn, a1137725141@163.com, fulj121@163.com, dlpeng@hdu.edu.cn, Lvqiang@hdu.edu.cn)

Jee Woong Choi is with the department of Marine Science and Convergence Engineering, Hanyang University, Ansan, 15588, Republic of Korea (e-mail:choijw@hanyang.ac.kr)

Alfonso Farina is with Selex-es (retired), consultant., Roma, 00144, Italy (e-mail:alfonso.farina@outlook.it)

This work was supported in part by the National Natural Science Foundation of China under Grant 62471165 and 61901151; in part by the Zhejiang Provincial Natural Science Foundation of China under Grant LZ23F030002. (Corresponding author: Dongliang Peng.)

under constraints on platform maneuver limitations (such as maximum acceleration and angular rate). To achieve radar trajectory control in real-time, existing literatures concentrate on the partially observed Markov Decision Process (POMDP) framework. This framework formulates the control decision-making problem as a first-order Markov process over time, and selects the best control commands via optimizing an objective function that quantitatively measures the goodness on the trajectory-control resulted estimation. This objective function can be either formulated into an information-driven reward as in [15]–[18], or a task-driven cost as in [19]–[24]. The optimal control commands are then obtained by either maximizing reward function or minimizing cost function. Nevertheless, it is noteworthy that both the reward and cost function in existing literatures necessities to implement pseudo tracking using predicted ideal measurement set (PIMS) that is generated by traversing all admissible radar trajectory control commands, and calculate posterior state estimates before actuating radar to its eventual state. This exhaustive enumeration operation inevitably leads to cumbersome computation. Furthermore, existing radar trajectory control literatures rarely investigate the fundamental impact of T2R geometry on the TMU and tracking accuracy, which in turn suppresses the benefits of radar trajectory optimization.

In this paper, we pay specific interests on radar tracking in clutter with T2R geometry-dependent TMU, and rigorously formulate the impact of T2R geometry on TMU and MSE lower bound. Three main contributions of this paper are summarized as follows:

- Derive the generalized form of target measurement error covariance for bistatic radar with moving receiver and transmitter illuminating any type of signal, and also give its approximated solution to specify the impact of T2R geometry on error covariance.
- Rigorously derive an improved PCRLB (IPCRLB) for radar tracking in clutter by fully accounting for radar measurement uncertainty in terms of both MOU and geometry-dependent TMU. The information gain factor (IGF) is specifically defined to quantify additional target Fisher information arising from considering dependence of target detection probability and measurement error covariance on T2R geometry. This factor reduces to zero when the dependence is completely ignored. The derived IPCRLB provides a much more accurate (less conservative) MSE lower bound compared to state-of-the-art bounds that partially or completely ignore the dependence of TMU on T2R geometry. Numerical investigation demonstrates the improvement of IPCRLB over existing bounds tends to enlarge as TMU increases.
- To leverage the superior IPCRLB to radar trajectory control, the trace of predictive IPCRLB is proposed as the cost function and minimized to optimize T2R geometry to acquire high-quality target measurement for improved radar tracking in clutter. Since IPCRLB fundamentally investigates the impact of T2R geometry on the MSE lower bound, compared to state-of-the-art control methods, proposed method optimizes T2R geometry more

effectively and exhibits least uncertainty of acquired target measurement and more accurate tracking results.

The organization of this paper: geometry-dependent TMU is formulated in section II. section III presents the detailed derivation of the proposed IPCRLB fully accounting for radar measurement uncertainty, followed by its application to radar trajectory control in section IV, section V validates proposed model and methods with simulation study, closed with conclusion in section V.

II. GEOMETRY-DEPENDENT TARGET MEASUREMENT UNCERTAINTY

The bistatic radar system consists of separately deployed transmitter and receiver, in which transmitter is dedicated to transmit certain type of signal towards to surveillance area, while the receiver is responsible for collecting and processing reflected signals. Either the transmitter or the receiver can be mounted to moving platform and is usually collaborative. The bistatic radar is a highly generalized radar system that coincides to be monostatic radar when the transmitter and receiver are collocated, or becomes a passive radar when the target serves as the illuminator. Without loss of generality, this section uses bistatic radar to demonstrate the impact of T2R geometry on the TMU. Unlike [25], [26]–[28], which are limited to static radar with specific signals, the geometry-dependent bistatic measurement error covariance formulated here is a much more generalized form. It can be used for bistatic radar tracking with moving receiver and transmitter illuminating any type of signal.

A. Bistatic radar overview

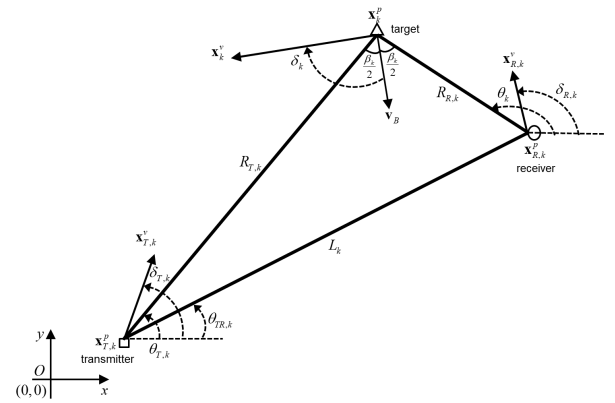


Fig. 1. Bistatic radar operation in 2D Cartesian coordinate

Instead of the specified north-referenced coordinate system [25], [26]–[28], we consider a more generalized two-dimensional (2D) Cartesian coordinate system to demonstrate bistatic radar operation for radar tracking with moving target, transmitter and receiver as shown in Fig.1. The full state of either moving target, transmitter or receiver composites of two-dimensional position and velocity, denoted by $\mathbf{x}_k = \left[\left(\mathbf{x}_k^p \right)^T \quad \left(\mathbf{x}_k^v \right)^T \right]^T$, $\mathbf{x}_{T,k} = \left[\left(\mathbf{x}_{T,k}^p \right)^T \quad \left(\mathbf{x}_{T,k}^v \right)^T \right]^T$ and

$\mathbf{x}_{R,k} = \left[\left(\mathbf{x}_{R,k}^p \right)^T \left(\mathbf{x}_{R,k}^v \right)^T \right]^T$, respectively. At each time t_k , the separately deployed target, transmitter and receiver form a bistatic triangular geometry that can be denoted by the abbreviation $\Delta_k \triangleq \Delta(\mathbf{x}_k^p, \mathbf{x}_{T,k}^p, \mathbf{x}_{R,k}^p)$. As shown in Fig.1, Δ_k can be described by a set of triangle parameters $(L_k, R_{T,k}, R_{R,k}, \theta_{TR,k}, \theta_{T,k}, \theta_k)$. L_k is the baseline range between transmitter and receiver, $R_{T,k}$ is the transmitter to target range, $R_{R,k}$ is the receiver to target range, with the target bistatic range defined by $d_k = R_{R,k} + R_{T,k}$. $\theta_{TR,k}$ is the angle of transmitter-to-receiver line-of-sight (LOS), $\theta_{T,k}$ and θ_k are the transmitter and receiver look angles respectively, both measured positive counter-clockwise from the x-axis and restricted to $[0, 2\pi]$. Among parameters above, $\theta_{TR,k}$ is used to locate the triangle in the 2D Cartesian space, while $(d_k, L_k, \theta_{T,k}, \theta_k)$ is used to uniquely determine the shape of the triangle. Obviously, this triangle Δ_k is time-varying that changes as any of target, transmitter and receiver moves along its trajectory, and converges to be a straight line when the target-transmitter-receiver becomes collinear or transmitter-receiver is collocated.

In bistatic radar system, the receiver cooperates with the transmitter to measure the time delay τ_k and Doppler shift ξ_k of received target echo, which are then converted to obtain the bistatic range d_k and bistatic velocity (bistatic range rate) v_k , while the direction-of-arrival (DOA) of target echo can be directly obtained as the receiver looking angle θ_k . Therefore, the target state \mathbf{x}_k can be recursively estimated based on the bistatic measurement $\mathbf{z}_k = [d_k \ v_k \ \theta_k]^T$. Relationship between bistatic measurement and target's state can be described by

$$\mathbf{z}_k = \mathbf{h}(\mathbf{x}_k) + \mathbf{w}_k, \quad (1)$$

where $\mathbf{h}(\mathbf{x}_k)$ is a time-invariant nonlinear vector function of target state \mathbf{x}_k , and composites of noise-free bistatic range, bistatic velocity and DOA given by

$$h^d(\mathbf{x}_k) = \|\mathbf{x}_k^p - \mathbf{x}_{T,k}^p\|_2 + \|\mathbf{x}_k^p - \mathbf{x}_{R,k}^p\|_2 \quad (2a)$$

$$h^v(\mathbf{x}_k) = \frac{(\mathbf{x}_k^p - \mathbf{x}_{T,k}^p)^T (\mathbf{x}_k^v - \mathbf{x}_{T,k}^v)}{\|\mathbf{x}_k^p - \mathbf{x}_{T,k}^p\|_2} + \frac{(\mathbf{x}_k^p - \mathbf{x}_{R,k}^p)^T (\mathbf{x}_k^v - \mathbf{x}_{R,k}^v)}{\|\mathbf{x}_k^p - \mathbf{x}_{R,k}^p\|_2} \quad (2b)$$

$$h^\theta(\mathbf{x}_k) = \tan^{-1} \frac{y_k - y_{R,k}}{x_k - x_{R,k}}, \quad (2c)$$

where $\|\cdot\|_2$ is the Euclidean norm, \mathbf{w}_k denotes the additive white Gaussian noise. The relationship between bistatic signal (τ_k, ξ_k) and bistatic measurement (d_k, v_k) can be described as follow

$$\tau_k = \frac{d_k}{c}, \xi_k = \frac{f_c}{c} v_k \quad (3)$$

where c and f_c are the speed of light and carrier frequency of transmitted signal, respectively. Since the derivation of T2R geometry-dependent error covariance in section II-B needs to calculate the derivative of ξ_k with respect to d_k , an alternative to formulate the Doppler shift ξ_k as a function of bistatic

range d_k is given by (derivation refers to Appendix A in supplementary material)

$$\xi_k = \frac{f_c}{c} \left[2\|\mathbf{x}_k^v\|_2 \cos \delta_k \cos \left(\frac{\beta_k}{2} \right) + \|\mathbf{x}_{T,k}^v\|_2 \cos(\delta_{T,k} - \theta_{T,k}) + \|\mathbf{x}_{R,k}^v\|_2 \cos(\delta_{R,k} - \theta_k) \right] \quad (4)$$

where δ_k is the angle measured from bisector vector \mathbf{v}_B to target velocity vector \mathbf{x}_k^v and restricted to $[0, 2\pi]$. $\delta_{T,k}$ and $\delta_{R,k}$ denote the angle of transmitter velocity vector $\mathbf{x}_{T,k}^v$ and receiver velocity vector $\mathbf{x}_{R,k}^v$, respectively, both measured positive counter-clockwise from the x-axis and restricted to $[0, 2\pi]$. β_k is the bistatic angle between transmitter and receiver with vertex at the target and $\cos\left(\frac{\beta_k}{2}\right)$ is calculated by

$$\cos\left(\frac{\beta_k}{2}\right) = \begin{cases} \frac{d_k + L_k \cos(\theta_k - \theta_{TR,k})}{\sqrt{d_k^2 + L_k^2 + 2d_k L_k \cos(\theta_k - \theta_{TR,k})}}, & \beta_k \neq \pi \\ 0, & \text{otherwise} \end{cases} \quad (5)$$

As shown in (4) and (5), the target Doppler frequency ξ_k is collectively determined by T2R relative position through triangular geometry parameters $(d_k, L_k, \theta_k, \theta_{TR,k})$, and target velocity \mathbf{x}_k^v , transmitter velocity $\mathbf{x}_{T,k}^v$, receiver velocity $\mathbf{x}_{R,k}^v$.

B. Geometry-dependent target measurement uncertainty

At each observation time t_k , bistatic radar randomly returns a target-originated measurement \mathbf{z}_k with detection probability less than one, and \mathbf{z}_k is corrupted by statistical noise \mathbf{w}_k that is usually modeled by white Gaussian with zero mean and covariance. Therefore, detection probability and error covariance collectively determine the TMU. More specifically, the higher the detection probability, the lower the uncertainty a radar returns a target measurement, while the smaller the error covariance, the less the uncertainty contained in target measurement. Reminder of this section concentrates on deriving the generalized form for TMU of bistatic radar, and giving an approximated solution to specify the impact of T2R geometry on measurement error covariance.

To keep consistence with existing work, the target is assumed to follow a Swerling I model, thus its detection probability depends on the T2R geometry through the signal-to-noise ratio (SNR) and can be calculated by [25]

$$P_d(\Delta_k) = P_{FA}^{1/(1+\Psi_k(\Delta_k))} \quad (6)$$

where P_{FA} is the false alarm rate and $\Psi_k(\Delta_k)$ is the SNR at the receiver. $\Psi_k(\Delta_k)$ is time-varying and depends on the T2R geometry Δ_k through the energy path-loss factor due to signal propagation, given by

$$\Psi_k(\Delta_k) = \frac{\vartheta_0^4}{(\|\mathbf{x}_k^p - \mathbf{x}_{T,k}^p\|_2 \|\mathbf{x}_k^p - \mathbf{x}_{R,k}^p\|_2)^2} = \frac{\vartheta_0^4}{(R_{T,k} R_{R,k})^2} \quad (7)$$

where ϑ_0 is the transmitted signal constant. As pointed out in [25], the error of DOA is inversely proportional to the SNR $\Psi_k(\Delta_k)$ at the receiver and independent to the errors of bistatic range and velocity, therefore the error covariance of target bistatic radar measurement \mathbf{z}_k can be approximated by its CRLB as

$$\begin{aligned} \mathbf{R}_k(\Delta_k) &\approx \text{diag}(\mathbf{C}(d_k, v_k), \mathbf{C}(\theta_k)) \\ &= \begin{bmatrix} [\mathbf{J}_M(d_k, v_k)]^{-1} & 0 \\ 0 & \frac{\sigma_{\theta_0}^2}{\Psi_k(\Delta_k)} \end{bmatrix} \end{aligned} \quad (8)$$

$$\mathbf{R}_k(\Delta_k) = \frac{1}{\Psi_k(\Delta_k)} \frac{c^4}{f_c^2(S_1 S_3 - S_2^2)} \begin{bmatrix} \left[\begin{array}{cc} \frac{f_c^2}{c^2} S_3 & -\frac{f_c}{c^2} S_2 - \frac{f_c}{c} \frac{\partial \xi_k}{\partial d_k} S_3 \\ -\frac{f_c}{c^2} S_2 - \frac{f_c}{c} \frac{\partial \xi_k}{\partial d_k} S_3 & \frac{1}{c^2} S_1 + \frac{2}{c} \frac{\partial \xi_k}{\partial d_k} S_2 + \left(\frac{\partial \xi_k}{\partial d_k} \right)^2 S_3 \end{array} \right] & 0 \\ 0 & \frac{\sigma_{\theta_0}^2 f_c^2 (S_1 S_3 - S_2^2)}{c^4} \end{bmatrix} \quad (14)$$

where σ_{θ_0} is the standard deviation of referred DOA signal, $\mathbf{C}(d_k, v_k)$ denotes the CRLB for bistatic range d_k and bistatic velocity v_k , and $\mathbf{C}(\theta_k)$ denotes the CRLB for DOA θ_k . $\mathbf{J}_M(d_k, v_k)$ is the FIM for d_k and v_k . Since the target bistatic measurement (d_k, v_k) is converted from its bistatic signal (τ_k, ξ_k) via (3) and (4), $\mathbf{J}_M(d_k, v_k)$ can be therefore obtained by transforming the FIM for (τ_k, ξ_k) in signal domain to measurement domain as [25], [14], [26]

$$\mathbf{J}_M(d_k, v_k) = \mathbf{P}_k \mathbf{J}_S(\tau_k, \xi_k) \mathbf{P}_k^T \quad (9)$$

where $\mathbf{J}_S(\tau_k, \xi_k)$ denotes the FIM for τ_k and ξ_k , and is determined by both the SNR $\Psi_k(\Delta_k)$ at the receiver and geometry-independent signal parameter [25], [26],

$$\mathbf{J}_S(\tau_k, \xi_k) = \Psi_k(\Delta_k) \begin{bmatrix} S_1 & S_2 \\ S_2 & S_3 \end{bmatrix} \quad (10)$$

with S_1, S_2, S_3 denoting constants related to transmitted signal. \mathbf{P}_k is the transformation matrix from the signal domain (τ_k, ξ_k) to measurement domain (d_k, v_k) , and depends on the states of both target and radar, given by

$$\mathbf{P}_k = \begin{bmatrix} \frac{\partial \tau_k}{\partial d_k} & \frac{\partial \tau_k}{\partial v_k} \\ \frac{\partial \xi_k}{\partial d_k} & \frac{\partial \xi_k}{\partial v_k} \end{bmatrix} \quad (11)$$

with each element calculated as

$$\frac{\partial \tau_k}{\partial d_k} = \frac{1}{c}, \frac{\partial \tau_k}{\partial v_k} = 0, \frac{\partial \xi_k}{\partial v_k} = \frac{f_c}{c} \quad (12)$$

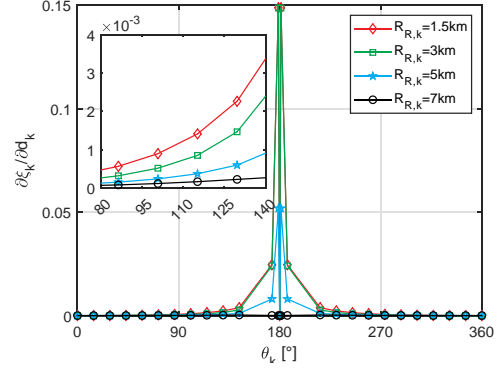
in particular, $\frac{\partial \xi_k}{\partial d_k}$ is given by

$$\frac{\partial \xi_k}{\partial d_k} = \begin{cases} \frac{f_c}{c} \frac{2\|\mathbf{x}_k^v\|_2 \cos \delta_k L_k^2 \sin^2(\theta_k - \theta_{TR,k})}{\sqrt{(d_k^2 + L_k^2 + 2d_k L_k \cos(\theta_k - \theta_{TR,k}))^3}}, \beta_k \neq \pi \\ 0, \text{ otherwise} \end{cases} \quad (13)$$

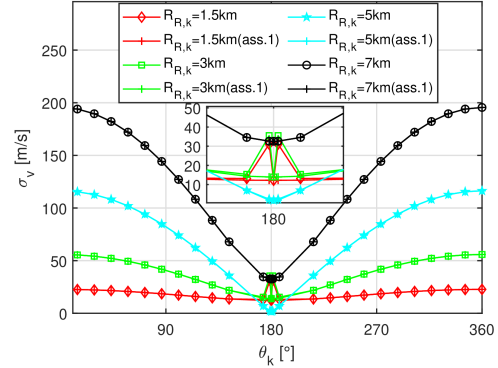
Substituting (10-11) to (9), whose result is then substituted to (8), the full expression of radar measurement error covariance can be finalized as shown in (14).

Remark 1: as seen in (14), $\mathbf{R}_k(\Delta_k)$ is collectively determined by three types of factors, i.e., SNR $\Psi_k(\Delta_k)$, $\frac{\partial \xi_k}{\partial d_k}$ and signal parameters (S_1, S_2, S_3) . Among these factors, (S_1, S_2, S_3) usually keeps fixed once transmitted signal is selected, while $\Psi_k(\Delta_k)$ depends on the T2R geometry Δ_k through term $R_{T,k} R_{R,k}$ shown in (7), and $\frac{\partial \xi_k}{\partial d_k}$ relates to both T2R geometry Δ_k through $(d_k, L_k, \theta_k, \theta_{TR,k})$ and target velocity \mathbf{x}_k^v as shown in (13), either $\Psi_k(\Delta_k)$ or $\frac{\partial \xi_k}{\partial d_k}$ changes as any of the target and radar moves along its trajectory. Therefore, in realistic radar operation, target measurement error covariance $\mathbf{R}_k(\Delta_k)$ is time varying and collectively affected by both T2R geometry Δ_k and target velocity \mathbf{x}_k^v .

Assumption 1: to simplify (14), we make an assumption $\frac{\partial \xi_k}{\partial d_k} \approx 0$ for any value of $\beta_k \neq \pi$, i.e., the target Doppler shift hardly changes as the bistatic range varies. The complicated expression in (13) hampers us to mathematically analyze the



(a) $\frac{\partial \xi_k}{\partial d_k}$ versus target DOA θ_k



(b) σ_v versus θ_k with and without assumption 1

Fig. 2. Numerical validation of feasibility of assumption 1

approximation bias caused by Assumption 1. Instead, we investigate approximation bias via numerical experiments, in which T2R geometry is set to change as either $R_{R,k}$ or θ_k varies when target moves along its trajectory, with experimental setup detailed in section V. As respectively shown in Fig. 2a and Fig. 2b, as long as $\theta_k \neq 180^\circ$, the value of $\frac{\partial \xi_k}{\partial d_k}$ approaches to zero and there is no nontrivial difference between σ_v with and without assumption 1. Fortunately, the target is barely collinear with transmitter and receiver in realistic tracking scenario, hence approximation bias of assumption 1 can be acceptable. Consequently, $\mathbf{R}_k(\Delta_k)$ becomes only relevant to the T2R geometry Δ_k under assumption 1 and can be simplified as

$$\mathbf{R}_k(\Delta_k) \approx \frac{1}{\Psi(\Delta_k)} \frac{c^4}{f_c^2(S_1 S_3 - S_2^2)} \times \begin{bmatrix} \left[\begin{array}{cc} \frac{f_c^2}{c^2} S_3 & -\frac{f_c}{c^2} S_2 \\ -\frac{f_c}{c^2} S_2 & \frac{1}{c^2} S_1 \end{array} \right] & 0 \\ 0 & \frac{\sigma_{\theta_0}^2 f_c^2 (S_1 S_3 - S_2^2)}{c^4} \end{bmatrix} \quad (15)$$

III. IMPROVED PCRLB FULLY ACCOUNTING FOR RADAR MEASUREMENT UNCERTAINTY

In this section, we rigorously derive an improved PCRLB (IPCRLB) for radar tracking in clutter by fully accounting for radar measurement uncertainty in terms of both MOU and geometry-dependent TMU. When deriving IPCRLB, the information gain factor (IGF) is specifically defined to quantify additional target Fisher information extracted from current measurements by considering the dependence of target detection probability and measurement error covariance on T2R geometry. Since derivation of IPCRLB involves taking differentiating with respect to target state \mathbf{x}_k , for simplicity, all geometry-related parameters are abbreviated as the function of \mathbf{x}_k at the rest of this paper, i.e., $P_d(\Delta_k) \triangleq P_d(\mathbf{x}_k)$, $\mathbf{R}_k(\Delta_k) \triangleq \mathbf{R}_k(\mathbf{x}_k)$ and $\Psi_k(\Delta_k) \triangleq \Psi_k(\mathbf{x}_k)$.

A. Derivation of IPCRLB

Define $\mathbf{Z}(k) = \{\mathbf{z}_k^1, \dots, \mathbf{z}_k^{m_k}\}$ as the set of origin-unknown measurements returned by radar at time t_k , \mathbf{z}_k^i is the i -th measurement of $\mathbf{Z}(k)$, $i = 1, \dots, m_k$, m_k is the cardinality of $\mathbf{Z}(k)$. \mathbf{z}_k^i can be originated from either target of interest or clutter. At each time t_k , the radar randomly returned the target-originated measurement with detection probability $P_d(\mathbf{x}_k)$, and returned target measurement is corrupted by white Gaussian noise with zero mean and covariance $\mathbf{R}_k(\mathbf{x}_k)$. Therefore, the likelihood of target measurement \mathbf{z}_k^i conditioned on \mathbf{x}_k can be described by a Gaussian

$$p(\mathbf{z}_k^i) \triangleq p(\mathbf{z}_k^i | \mathbf{x}_k) = \frac{\exp\left[-\frac{1}{2}(\mathbf{z}_k^i - \mathbf{h}(\mathbf{x}_k))^T \mathbf{R}_k^{-1}(\mathbf{x}_k) (\mathbf{z}_k^i - \mathbf{h}(\mathbf{x}_k))\right]}{\sqrt{(2\pi)^n |\mathbf{R}_k(\mathbf{x}_k)|}} \quad (16)$$

where n is the dimension of \mathbf{z}_k^i . The number of clutter measurements in $\mathbf{Z}(k)$ is assumed to follow a Poisson distribution with mean number λV , with each clutter measurement is uniformly distributed over the radar measurement volume V with spatial density $\lambda = N_{cell} P_{FA} / V$, N_{cell} is the total number of radar resolution cells. Consequently, the probability that radar returns m_k measurements at time t_k can be calculated by [7], [12]- [25]

$$P(\mathbf{x}_k, m_k) = [1 - P_d(\mathbf{x}_k)] e^{-\lambda V} \frac{(\lambda V)^{m_k}}{m_k!} + P_d(\mathbf{x}_k) e^{-\lambda V} \frac{(\lambda V)^{m_k-1}}{(m_k-1)!} \quad (17)$$

The probability that there is one measurement in $\mathbf{Z}(k)$ originated from target with state \mathbf{x}_k can be described by [7], [12]- [25]

$$d(\mathbf{x}_k, m_k) = \frac{P_d(\mathbf{x}_k)}{(1 - P_d(\mathbf{x}_k)) \frac{\lambda V}{m_k} + P_d(\mathbf{x}_k)} \quad (18)$$

The likelihood of measurements $\mathbf{Z}(k)$ conditioned on target state \mathbf{x}_k and number of measurements m_k is given by [7], [12]- [25]

$$p(\mathbf{Z}(k) | \mathbf{x}_k, m_k) = \frac{1 - d(\mathbf{x}_k, m_k)}{V^{m_k}} + \frac{d(\mathbf{x}_k, m_k)}{m_k V^{m_k-1}} \sum_{i=1}^{m_k} p(\mathbf{z}_k^i) \quad (19)$$

Let \mathbf{J}_k denote the FIM for target state \mathbf{x}_k at t_k , its inverse is defined as the PCRLB that bounds the MSE of any unbiased estimator [1]

$$\mathbf{J}_k^{-1} \leq \mathbb{E}_{\mathbf{x}_k} \{(\hat{\mathbf{x}}_{k|k} - \mathbf{x}_k)(\hat{\mathbf{x}}_{k|k} - \mathbf{x}_k)^T\} \quad (20)$$

where $\mathbb{E}\{\cdot\}$ is the expectation operator. The Riccati-like recursion form to calculate \mathbf{J}_k is given by [2]

$$\mathbf{J}_k = (\mathbf{Q}_k + \mathbf{F}_k \mathbf{J}_{k-1}^{-1} \mathbf{F}_k^T)^{-1} + \mathbf{J}_k^Z \quad (21)$$

with \mathbf{F}_k and \mathbf{Q}_k denotes the target state propagation matrix and process noise covariance, respectively. The FIM in (21) consists of two parts: the target prior information up to time t_{k-1} and the target new information contributed by measurement $\mathbf{Z}(k)$ received at t_k . The new information \mathbf{J}_k^Z is defined and calculated as [7], [12]- [25]

$$\begin{aligned} \mathbf{J}_k^Z &= \mathbb{E}_{\mathbf{x}_k} \{ \{ \mathbb{E}_{m_k} \{ \mathbf{J}_k^Z(\mathbf{x}_k, m_k) \} \} \} \\ &= \mathbb{E}_{\mathbf{x}_k} \left\{ \sum_{m_k=1}^{\infty} P(\mathbf{x}_k, m_k) \mathbf{J}_k^Z(\mathbf{x}_k, m_k) \right\} \end{aligned} \quad (22)$$

where $\mathbf{J}_k^Z(\mathbf{x}_k, m_k)$ is the conditional measurement information matrix and defined as

$$\begin{aligned} \mathbf{J}_k^Z(\mathbf{x}_k, m_k) &= \mathbb{E}_{\mathbf{Z}(k)} \left\{ [\nabla_{\mathbf{x}_k} \ln p(\mathbf{Z}(k) | \mathbf{x}_k, m_k)] [\nabla_{\mathbf{x}_k} \ln p(\mathbf{Z}(k) | \mathbf{x}_k, m_k)]^T \right\} \end{aligned} \quad (23)$$

where $\nabla_{\mathbf{x}_k}$ denotes the first-order partial derivative operator with respect to \mathbf{x}_k . In particular, we treat both P_d and \mathbf{R}_k in $\ln p(\mathbf{Z}(k) | \mathbf{x}_k, m_k)$ as target state \mathbf{x}_k dependent parameters, and take the first-order partial derivative of the logarithm function of (19) w.r.t. \mathbf{x}_k . For simplicity, we follow [5]-[7], [25] to assume $\mathbf{R}_k(\mathbf{x}_k) = \text{diag}(\sigma_1^2, \dots, \sigma_n^2)$, consequently, $\nabla_{\mathbf{x}_k} \ln p(\mathbf{Z}(k) | \mathbf{x}_k, m_k)$ can be calculated and decomposed into three parts

$$\nabla_{\mathbf{x}_k} \ln p(\mathbf{Z}(k) | \mathbf{x}_k, m_k) = \mathbf{A} + \mathbf{B} + \mathbf{C} \quad (24)$$

with \mathbf{A} , \mathbf{B} , \mathbf{C} given by

$$\mathbf{A} = \frac{d(\mathbf{x}_k, m_k) \mathbf{H}_k^T(\mathbf{x}_k) \mathbf{R}_k^{-1}(\mathbf{x}_k)}{m_k V^{m_k-1} p(\mathbf{Z}(k) | \mathbf{x}_k, m_k)} \sum_{i=1}^{m_k} p(\mathbf{z}_k^i) [\mathbf{z}_k^i - \mathbf{h}(\mathbf{x}_k)] \quad (25)$$

$$\mathbf{B} = \frac{1}{p(\mathbf{Z}(k) | \mathbf{x}_k, m_k)} \left[\frac{\sum_{i=1}^{m_k} p(\mathbf{z}_k^i)}{m_k V^{m_k-1}} - \frac{1}{V^{m_k}} \right] \frac{\partial d(\mathbf{x}_k, m_k)}{\partial \mathbf{x}_k} \quad (26)$$

$$\begin{aligned} \mathbf{C} &= \frac{-d(\mathbf{x}_k, m_k)}{2 \Psi_k(\mathbf{x}_k) m_k V^{m_k-1} p(\mathbf{Z}(k) | \mathbf{x}_k, m_k)} \frac{\partial \Psi_k(\mathbf{x}_k)}{\partial \mathbf{x}_k} \times \\ &\sum_{i=1}^{m_k} p(\mathbf{z}_k^i) \left\{ [\mathbf{z}_k^i - \mathbf{h}(\mathbf{x}_k)]^T \mathbf{R}_k^{-1}(\mathbf{x}_k) [\mathbf{z}_k^i - \mathbf{h}(\mathbf{x}_k)] - n \right\} \end{aligned} \quad (27)$$

where $\mathbf{H}_k(\mathbf{x}_k)$ is the Jacobian matrix of measurement function $\mathbf{h}(\mathbf{x}_k)$. Please note, compared to existing work that treats both P_d and \mathbf{R}_k as state-independent parameters when taking the partial derivative of $\ln p(\mathbf{Z}(k) | \mathbf{x}_k, m_k)$ w.r.t. \mathbf{x}_k , the result in (24) contains two more terms, i.e., \mathbf{B} and \mathbf{C} . In particular, \mathbf{B} results from treating P_d as state-dependent parameter while \mathbf{C} results from treating \mathbf{R}_k as state-dependent parameter when

$$\begin{aligned} \mathbf{J}_k^{\mathbf{Z}}(\mathbf{x}_k, m_k) &= \mathbb{E}_{\mathbf{Z}(k)} \{ (\mathbf{A}\mathbf{A}^T + \mathbf{A}\mathbf{B}^T + \mathbf{A}\mathbf{C}^T + \mathbf{B}\mathbf{A}^T + \mathbf{B}\mathbf{B}^T + \mathbf{B}\mathbf{C}^T + \mathbf{C}\mathbf{A}^T + \mathbf{C}\mathbf{B}^T + \mathbf{C}\mathbf{C}^T) \} \\ &= \int_{\mathbf{z}_k^1 \in \Xi} \cdots \int_{\mathbf{z}_k^{m_k} \in \Xi} (\mathbf{A}\mathbf{A}^T + \mathbf{A}\mathbf{B}^T + \mathbf{A}\mathbf{C}^T + \mathbf{B}\mathbf{A}^T + \mathbf{B}\mathbf{B}^T + \mathbf{B}\mathbf{C}^T + \mathbf{C}\mathbf{A}^T + \mathbf{C}\mathbf{B}^T + \mathbf{C}\mathbf{C}^T) p(\mathbf{Z}(k) | \mathbf{x}_k, m_k) d\mathbf{z}_k^1 \cdots d\mathbf{z}_k^{m_k} \end{aligned} \quad (30)$$

$$\mathbf{J}_k^{\mathbf{Z}}(\mathbf{x}_k, m_k) = \int_{\tilde{\mathbf{z}}_k^1 \in \tilde{\Xi}} \cdots \int_{\tilde{\mathbf{z}}_k^{m_k} \in \tilde{\Xi}} \{ \mathbf{A}\mathbf{A}^T + \mathbf{B}\mathbf{B}^T + 2\mathbf{B}\mathbf{C}^T + \mathbf{C}\mathbf{C}^T \} p(\tilde{\mathbf{Z}}(k) | \mathbf{x}_k, m_k) d\tilde{\mathbf{z}}_k^1 \cdots d\tilde{\mathbf{z}}_k^{m_k} \quad (33)$$

differentiating $\ln p(\mathbf{Z}(k) | \mathbf{x}_k, m_k)$ w.r.t \mathbf{x}_k . Taking the first-order partial derivative of (18) and (7) w.r.s. to \mathbf{x}_k , respectively, we have

$$\frac{\partial d(\mathbf{x}_k, m_k)}{\partial \mathbf{x}_k} = \frac{-\lambda V m_k P_{\text{FA}}^{1/(1+\Psi_k(\mathbf{x}_k))}}{\{ [1 - P_d(\mathbf{x}_k)] \lambda V + m_k P_d(\mathbf{x}_k) \}^2} \times \frac{\ln P_{\text{FA}}}{[1 + \Psi_k(\mathbf{x}_k)]^2} \frac{\partial \Psi_k(\mathbf{x}_k)}{\partial \mathbf{x}_k} \quad (28)$$

$$\begin{aligned} \frac{\partial \Psi_k(\mathbf{x}_k)}{\partial \mathbf{x}_k} &= \frac{-2R_0^4}{R_{R,k}^4 R_{T,k}^4} \\ &\times \left[\left(\left[(\mathbf{x}_k^p - \mathbf{x}_{R,k}^p) \quad (\mathbf{x}_k^p - \mathbf{x}_{T,k}^p) \right] \begin{bmatrix} R_{T,k}^2 \\ R_{R,k}^2 \end{bmatrix} \right)^T \mathbf{0}_{1 \times 2} \right]^T \end{aligned} \quad (29)$$

By substituting (24) to (23), $\mathbf{J}_k^{\mathbf{Z}}(\mathbf{x}_k, m_k)$ can be then written as (30). Ξ in (30) denotes the integration region of \mathbf{z}_k^i , $i = 1, \dots, m_k$, the volume of Ξ is V . If we make the following change of variable:

$$\tilde{\mathbf{z}}_k^i = \mathbf{z}_k^i - \mathbf{h}(\mathbf{x}_k), \quad \tilde{\mathbf{z}}_k^i \in \tilde{\Xi} \quad (31)$$

$\tilde{\Xi}$ is the mapping of Ξ and becomes symmetric domain under the above transformation, the volume of $\tilde{\Xi}$ is still V , let $\tilde{\mathbf{Z}}(k) = \{ \tilde{\mathbf{z}}_k^1, \dots, \tilde{\mathbf{z}}_k^{m_k} \}$. Since $\tilde{\mathbf{z}}_k^i$ is an odd symmetric function of itself, while $[\tilde{\mathbf{z}}_k^i]^T \mathbf{R}_k^{-1}(\mathbf{x}_k) \tilde{\mathbf{z}}_k^i$ is an even symmetric function of $\tilde{\mathbf{z}}_k^i$, therefore, \mathbf{A} is an odd symmetric function of $\tilde{\mathbf{z}}_k^i$, whereas, both \mathbf{B} , \mathbf{C} and $p(\tilde{\mathbf{Z}}(k) | \mathbf{x}_k, m_k)$ become even symmetric functions of $\tilde{\mathbf{z}}_k^i$ for $i = 1, \dots, m_k$. Integrating an odd symmetric function over a symmetric domain $\tilde{\Xi}$, we have

$$\begin{cases} \int_{\tilde{\mathbf{z}}_k^1 \in \tilde{\Xi}} \cdots \int_{\tilde{\mathbf{z}}_k^{m_k} \in \tilde{\Xi}} \mathbf{A}\mathbf{B}^T p(\tilde{\mathbf{Z}}(k) | \mathbf{x}_k, m_k) d\tilde{\mathbf{z}}_k^1 \cdots d\tilde{\mathbf{z}}_k^{m_k} = 0 \\ \int_{\tilde{\mathbf{z}}_k^1 \in \tilde{\Xi}} \cdots \int_{\tilde{\mathbf{z}}_k^{m_k} \in \tilde{\Xi}} \mathbf{B}\mathbf{A}^T p(\mathbf{Z}(k) | \mathbf{x}_k, m_k) d\tilde{\mathbf{z}}_k^1 \cdots d\tilde{\mathbf{z}}_k^{m_k} = 0 \\ \int_{\tilde{\mathbf{z}}_k^1 \in \tilde{\Xi}} \cdots \int_{\tilde{\mathbf{z}}_k^{m_k} \in \tilde{\Xi}} \mathbf{A}\mathbf{C}^T p(\tilde{\mathbf{Z}}(k) | \mathbf{x}_k, m_k) d\tilde{\mathbf{z}}_k^1 \cdots d\tilde{\mathbf{z}}_k^{m_k} = 0 \\ \int_{\tilde{\mathbf{z}}_k^1 \in \tilde{\Xi}} \cdots \int_{\tilde{\mathbf{z}}_k^{m_k} \in \tilde{\Xi}} \mathbf{C}\mathbf{A}^T p(\tilde{\mathbf{Z}}(k) | \mathbf{x}_k, m_k) d\tilde{\mathbf{z}}_k^1 \cdots d\tilde{\mathbf{z}}_k^{m_k} = 0 \end{cases} \quad (32)$$

Hence, based on the above results, along with the fact $\mathbf{B}\mathbf{C}^T = \mathbf{C}\mathbf{B}^T$, (30) can be simplified as (33). Then substitute (25) - (27) to (33), we further have

$$\begin{aligned} \mathbf{J}_k^{\mathbf{Z}}(\mathbf{x}_k, m_k) &= \underbrace{\mathbf{H}_k^T(\mathbf{x}_k) \mathbf{A}_k^1(\mathbf{x}_k, m_k) \mathbf{R}_k^{-1}(\mathbf{x}_k) \mathbf{H}_k(\mathbf{x}_k)}_{\mathbb{E}_{\tilde{\mathbf{Z}}(k)} \{ \mathbf{A}\mathbf{A}^T \}} \\ &+ \underbrace{\mathbf{A}_k^2(\mathbf{x}_k, m_k) \frac{\partial \Psi_k(\mathbf{x}_k)}{\partial \mathbf{x}_k} \left[\frac{\partial \Psi_k(\mathbf{x}_k)}{\partial \mathbf{x}_k} \right]^T}_{\mathbb{E}_{\tilde{\mathbf{Z}}(k)} \{ \mathbf{B}\mathbf{B}^T + 2\mathbf{B}\mathbf{C}^T + \mathbf{C}\mathbf{C}^T \}} \end{aligned} \quad (34)$$

where matrix $\mathbf{A}_k^1(\mathbf{x}_k, m_k)$ is given by

$$\begin{aligned} \mathbf{A}_k^1(\mathbf{x}_k, m_k) &= \mathbb{E}_{\tilde{\mathbf{Z}}(k)} \left\{ \frac{d^2(\mathbf{x}_k, m_k) \mathbf{R}_k^{-1}(\mathbf{x}_k)}{m_k^2 V^{2m_k-2} p^2(\tilde{\mathbf{Z}}(k) | \mathbf{x}_k, m_k)} \right. \\ &\quad \left. \times \sum_{i=1}^{m_k} \sum_{j=1}^{m_k} p(\tilde{\mathbf{z}}_k^i) \tilde{\mathbf{z}}_k^i p(\tilde{\mathbf{z}}_k^j) (\tilde{\mathbf{z}}_k^j)^T \right\} \end{aligned} \quad (35)$$

and scalar $\mathbf{A}_k^2(\mathbf{x}_k, m_k)$ is defined by

$$\mathbf{A}_k^2(\mathbf{x}_k, m_k) = \mathbb{E}_{\tilde{\mathbf{Z}}(k)} \{ (\Gamma_{\mathbf{B}\mathbf{B}^T} + \Gamma_{\mathbf{B}\mathbf{C}^T} + \Gamma_{\mathbf{C}\mathbf{C}^T}) \} \quad (36)$$

with

$$\begin{aligned} \Gamma_{\mathbf{B}\mathbf{B}^T} &= \frac{\lambda^2 V^2 m_k^2 P_{\text{FA}}^{2/(1+\Psi_k(\mathbf{x}_k))}}{\{ [1 - P_d(\mathbf{x}_k)] \lambda V + m_k P_d(\mathbf{x}_k) \}^4} \\ &\times \frac{\ln^2 P_{\text{FA}}}{[1 + \Psi_k(\mathbf{x}_k)]^4} \frac{1}{p^2(\tilde{\mathbf{Z}}(k) | \mathbf{x}_k, m_k)} \\ &\times \left[\frac{\sum_{i=1}^{m_k} p(\tilde{\mathbf{z}}_k^i)}{m_k V^{m_k-1}} - \frac{1}{V^{m_k}} \right] \left[\frac{\sum_{j=1}^{m_k} p(\tilde{\mathbf{z}}_k^j)}{m_k V^{m_k-1}} - \frac{1}{V^{m_k}} \right] \end{aligned} \quad (37)$$

$$\begin{aligned} \Gamma_{\mathbf{B}\mathbf{C}^T} &= \frac{d(\mathbf{x}_k, m_k)}{\Psi_k(\mathbf{x}_k) V^{m_k-2}} \frac{\ln P_{\text{FA}}}{[1 + \Psi_k(\mathbf{x}_k)]^2} \\ &\times \frac{\lambda P_{\text{FA}}^{1/(1+\Psi_k(\mathbf{x}_k))}}{\{ [1 - P_d(\mathbf{x}_k)] \lambda V + m_k P_d(\mathbf{x}_k) \}^2} \frac{1}{p^2(\tilde{\mathbf{Z}}(k) | \mathbf{x}_k, m_k)} \\ &\times \left[\frac{\sum_{i=1}^{m_k} p(\tilde{\mathbf{z}}_k^i)}{m_k V^{m_k-1}} - \frac{1}{V^{m_k}} \right] \sum_{j=1}^{m_k} p(\tilde{\mathbf{z}}_k^j) \left\{ (\tilde{\mathbf{z}}_k^j)^T \mathbf{R}_k^{-1}(\mathbf{x}_k) \tilde{\mathbf{z}}_k^j - n \right\} \end{aligned} \quad (38)$$

$$\begin{aligned} \Gamma_{\mathbf{C}\mathbf{C}^T} &= \frac{d^2(\mathbf{x}_k, m_k)}{4\Psi^2(\mathbf{x}_k) m_k^2 V^{2m_k-2}} \sum_{i=1}^{m_k} p(\tilde{\mathbf{z}}_k^i) \left\{ (\tilde{\mathbf{z}}_k^i)^T \mathbf{R}_k^{-1}(\mathbf{x}_k) \tilde{\mathbf{z}}_k^i - n \right\} \\ &\times \frac{1}{p^2(\tilde{\mathbf{Z}}(k) | \mathbf{x}_k, m_k)} \sum_{j=1}^{m_k} p(\tilde{\mathbf{z}}_k^j) \left\{ (\tilde{\mathbf{z}}_k^j)^T \mathbf{R}_k^{-1}(\mathbf{x}_k) \tilde{\mathbf{z}}_k^j - n \right\} \end{aligned} \quad (39)$$

Note that, the first term on the right hand side of $\mathbf{J}_k^{\mathbf{Z}}(\mathbf{x}_k, m_k)$ shown in (34) is obtained by taking expectation of $\mathbf{A}\mathbf{A}^T$ w.r.t. $\tilde{\mathbf{Z}}(k)$, whose form is exactly the same as [5]–[7], [25] that only consider the MOU and totally ignore the geometry-dependent TMU when differentiating $\ln p(\mathbf{Z}(k) | \mathbf{x}_k, m_k)$ w.r.t \mathbf{x}_k . While, the second term in (34) is obtained by taking expectation of $\mathbf{B}\mathbf{B}^T + 2\mathbf{B}\mathbf{C}^T + \mathbf{C}\mathbf{C}^T$ w.r.t. $\tilde{\mathbf{Z}}(k)$, and acts as the additional conditional measurement information matrix stemmed from specifically treating both P_d and \mathbf{R}_k state-dependent parameters when differentiating $\ln p(\mathbf{Z}(k) | \mathbf{x}_k, m_k)$ w.r.t \mathbf{x}_k . To further calculate the conditional measurement information matrix derived in (34),

$$\Lambda_k^2(\mathbf{x}_k, m_k) = |\mathbf{R}_k(\mathbf{x}_k)|^{m_k/2} \int_{-g}^g \cdots \int_{-g}^g \cdots \int_{-g}^g \frac{(\Upsilon_1 + \Upsilon_2 + \Upsilon_3)}{\beta(\mathbf{x}_k, m_k)} d\tilde{\mathbf{z}}_k^1[1] \cdots d\tilde{\mathbf{z}}_k^1[n] \cdots d\tilde{\mathbf{z}}_k^{m_k}[1] \cdots d\tilde{\mathbf{z}}_k^{m_k}[n] \quad (43)$$

$$\Upsilon_1 = \frac{\lambda^2 V_g^2 m_k^2 (P_{FA}^g)^{2/(1+\Psi_k(\mathbf{x}_k))} \ln^2 P_{FA}^g}{\ell_g^4 [1 + \Psi_k(\mathbf{x}_k)]^4} \left\{ \frac{e^{-\sum_{h=1}^n (\tilde{\mathbf{z}}_k^1[h])^2} + (m_k - 1) e^{-\frac{\sum_{h=1}^n (\tilde{\mathbf{z}}_k^1[h])^2 + (\tilde{\mathbf{z}}_k^2[h])^2}{2}}}{m_k V_g^{2m_k - 2} (2\pi)^n |\mathbf{R}_k(\mathbf{x}_k)|} - \frac{2e^{-\frac{\sum_{h=1}^n (\tilde{\mathbf{z}}_k^1[h])^2}{2}}}{V_g^{2m_k - 1} \sqrt{(2\pi)^n |\mathbf{R}_k(\mathbf{x}_k)|}} + \frac{1}{V_g^{2m_k}} \right\} \quad (44)$$

one needs to deal with complicated expectations w.r.t. $\tilde{\mathbf{Z}}(\mathbf{k})$ appeared in (35) and (36). To keep consistence with [5]–[7], [25], the followed assumption is made to simplify the calculation of (35) and (36).

Assumption 2: since the "far out" measurements will be given very small weight when using a reasonable data association algorithm, measurements are restricted to a validation gate of size g times standard deviations, i.e.,

$$|\tilde{\mathbf{z}}_k^i[h]| = |\mathbf{z}_k^i[h] - \mathbf{h}^h(\mathbf{x}_k)| < g\sigma_h, \quad h = 1, \dots, n \quad (40)$$

with $\tilde{\mathbf{z}}_k^i = [\tilde{\mathbf{z}}_k^i[1] \cdots \tilde{\mathbf{z}}_k^i[n]]^T$, $\tilde{\mathbf{z}}_k^i[h]$ denotes the h -th component of measurement $\tilde{\mathbf{z}}_k^i$, and σ_h is the standard deviation of h -th component of $\tilde{\mathbf{z}}_k^i$. In the bistatic radar system introduced in section II, $n = 3$, corresponding to the bistatic range, bistatic velocity and DOA, respectively.

Assumption 3: the measurement dimensions are assumed to be orthogonal. This assumption gives good approximation for small integral regions, which can be described by n -dimensional cube:

$$\hat{\Xi} = [-g\sigma_1, g\sigma_1] \times \cdots \times [-g\sigma_n, g\sigma_n] \quad (41)$$

with its corresponding volume:

$$V_g = (2g)^n \prod_{h=1}^n \sigma_h \quad (42)$$

Note that the typical value of g is usually set to be 3 or 4, which means the probability that a target-generated measurement falling inside the validation gate is nearly one, therefore, the target detection probability inside the gate denoted by $P_d^g(\mathbf{x}_k)$ is almost equal to target detection probability $P_d(\mathbf{x}_k)$, i.e., $P_d^g(\mathbf{x}_k) \approx P_d(\mathbf{x}_k)$. Similarly, other parameters can also be reasonably approximated inside gate, i.e., $P_{FA}^g \approx P_{FA}$, $P_g(\mathbf{x}_k, m_k) \approx P(\mathbf{x}_k, m_k)$, and $d_g(\mathbf{x}_k, m_k) \approx d(\mathbf{x}_k, m_k)$. Based upon these considerations, we derive $\Lambda_k^2(\mathbf{x}_k, m_k)$ in Appendix B in supplementary material, and its final result is given in (43), in which $\tilde{\mathbf{z}}_k^i[h] = \mathbf{z}_k^i[h] / \sigma_h$, $h = 1, \dots, n$, and parameters Υ_1 , Υ_2 and Υ_3 are calculated by (44)–(46), respectively. Since $\Lambda_k^1(\mathbf{x}_k, m_k)$ is exactly the same information reduction factor (IRF) as existing bound, we directly use the final equation from [5]–[7], [25]:

$$\Lambda_k^1(\mathbf{x}_k, m_k) = \Lambda_k^1(\mathbf{x}_k, m_k) \times \mathbf{I}_n \quad (47)$$

where \mathbf{I}_n is the identity matrix with dimension n , $\Lambda_k^1(\mathbf{x}_k, m_k)$ is calculated by (48), with $\beta(\mathbf{x}_k, m_k)$ given by

$$\beta(\mathbf{x}_k, m_k) = \frac{1 - d_g(\mathbf{x}_k, m_k)}{V_g^{m_k}} + \frac{d_g(\mathbf{x}_k, m_k)}{V_g^{m_k - 1} \sqrt{(2\pi)^n |\mathbf{R}_k(\mathbf{x}_k)|}} e^{-\frac{\sum_{h=1}^n (\tilde{\mathbf{z}}_k^1[h])^2}{2}} \quad (49)$$

Note that, to solve the integral involved in (43) and (48), we follow [5]–[7], [25], and utilize the principle of importance sampling to carry out a Monte Carlo approximation, i.e., drawing sufficient realizations of each independently and identically distributed random variable $\tilde{\mathbf{z}}_k^i[n]$ from a uniform distribution in $[-g, g]$. Furthermore, the sum on the right hand side of (22) goes from one to infinity, for simplicity, the sum can be truncated to a small m_k , such as, $m_k = 2$ or 3, its approximation error can be negligible when the false alarm rate is low. Another critical problem to calculate (22) comes to the expectation operator taken with respect to state vector \mathbf{x}_k . This calculation can be performed off-line via Monte Carlo simulation by generating a set of target trajectory realizations and then calculating the averaged value. Another straightforward way is to use the mean value of the estimate of \mathbf{x}_k .

B. Information gain factor arising from geometry-dependent target measurement uncertainty

As shown in (34), $\mathbf{J}_k^Z(\mathbf{x}_k, m_k)$ contains two parts: the first part is conventional information matrix $\mathbf{H}_k^T(\mathbf{x}_k) \mathbf{R}_k^{-1}(\mathbf{x}_k) \mathbf{H}_k(\mathbf{x}_k)$ weighted by IRF $\Lambda_k^1(\mathbf{x}_k, m_k)$ to account for MOU, its form is exactly the same as existing PCRLBs in [5]–[7], [25]. The other part is the additional information matrix $\frac{\partial \Psi(\mathbf{x}_k)}{\partial \mathbf{x}_k} \left[\frac{\partial \Psi(\mathbf{x}_k)}{\partial \mathbf{x}_k} \right]^T$ weighted by $\Lambda_k^2(\mathbf{x}_k, m_k)$, which quantifies the additional target Fisher information extracted from current measurements $\mathbf{Z}(k)$ due to the geometry-dependent TMU. Considering the second part in (34) is essentially additional target Fisher information arising from geometry-dependent TMU, we define $\Lambda_k^2(\mathbf{x}_k, m_k)$ as the information gain factor (IGF) to highlight the positive impact of considering dependence of TMU on T2R geometry when differentiating $\ln p(\mathbf{Z}(k) | \mathbf{x}_k, m_k)$ w.r.t \mathbf{x}_k .

The conditional measurement information matrix derived in (34) is actually a generalized form that fully accounts for both MOU and geometry-dependent TMU. If we neglect the geometry-dependent TMU and treat both P_d and \mathbf{R}_k as state-independent parameters when differentiating $\ln p(\mathbf{Z}(k) | \mathbf{x}_k, m_k)$ w.r.t \mathbf{x}_k , both \mathbf{B} and \mathbf{C} in (24) become zero matrices, hence $\Lambda_k^2(\mathbf{x}_k, m_k)$ in (36) equals to zero and the entire second part in (34) vanishes. Hence, $\mathbf{J}_k^Z(\mathbf{x}_k, m_k)$ in

$$\Upsilon_2 = \frac{d_g(\mathbf{x}_k, m_k)}{\Psi_k(\mathbf{x}_k) V_g^{m_k-2}} \frac{\lambda(P_{\text{FA}}^g)^{1/(1+\Psi_k(\mathbf{x}_k))} \ln P_{\text{FA}}^g}{\ell_g^2 [1 + \Psi_k(\mathbf{x}_k)]^2} \times \left\{ \frac{e^{-\sum_{h=1}^n (\hat{z}_k^1[h])^2} \left[\sum_{h=1}^n (\hat{z}_k^1[h])^2 - n \right] + (m_k - 1) e^{-\frac{\sum_{h=1}^n (\hat{z}_k^1[h])^2 + \sum_{h=1}^n (\hat{z}_k^2[h])^2}{2}} \left[\sum_{h=1}^n (\hat{z}_k^2[h])^2 - n \right]}{V_g^{m_k-1} (2\pi)^n |\mathbf{R}_k(\mathbf{x}_k)|} - \frac{m_k e^{-\frac{\sum_{h=1}^n (\hat{z}_k^1[h])^2}{2}} \left[\sum_{h=1}^n (\hat{z}_k^1[h])^2 - n \right]}{V_g^{m_k} \sqrt{(2\pi)^n |\mathbf{R}_k(\mathbf{x}_k)|}} \right\} \quad (45)$$

$$\Upsilon_3 = \frac{d_g^2(\mathbf{x}_k, m_k)}{4\Psi_k^2(\mathbf{x}_k) m_k^2 V_g^{2m_k-2} (2\pi)^n |\mathbf{R}_k(\mathbf{x}_k)|} \times \left\{ m_k (m_k - 1) e^{-\frac{\sum_{h=1}^n (\hat{z}_k^1[h])^2 + (\hat{z}_k^2[h])^2}{2}} \left[\sum_{h=1}^n (\hat{z}_k^1[h])^2 - n \right] \left[\sum_{h=1}^n (\hat{z}_k^2[h])^2 - n \right] + m_k e^{-\sum_{h=1}^n (\hat{z}_k^1[h])^2} \left[\sum_{h=1}^n (\hat{z}_k^1[h])^2 - n \right]^2 \right\} \quad (46)$$

$$\Lambda_k^1(\mathbf{x}_k, m_k) = \frac{d_g^2(\mathbf{x}_k, m_k) |\mathbf{R}_k(\mathbf{x}_k)|^{(m_k-2)/2}}{m_k V_g^{2m_k-2} (2\pi)^n} \int_{-g}^g \cdots \int_{-g}^g \cdots \int_{-g}^g \cdots \int_{-g}^g \frac{(\hat{z}_k^1[1])^2 e^{-\sum_{h=1}^n (\hat{z}_k^1[h])^2}}{\beta(\mathbf{x}_k, m_k)} d\hat{z}_k^1[1] \cdots d\hat{z}_k^1[n] \cdots d\hat{z}_k^{m_k}[1] \cdots d\hat{z}_k^{m_k}[n] \quad (48)$$

$$\Lambda_k^2(\mathbf{x}_k, m_k) = |\mathbf{R}_k(\mathbf{x}_k)|^{m_k/2} \int_{-g}^g \cdots \int_{-g}^g \cdots \int_{-g}^g \cdots \int_{-g}^g \frac{\Upsilon_1}{\beta(\mathbf{x}_k, m_k)} d\hat{z}_k^1[1] \cdots d\hat{z}_k^1[n] \cdots d\hat{z}_k^{m_k}[1] \cdots d\hat{z}_k^{m_k}[n] \quad (51)$$

(34) reduces to the conventional form of existing PCRLBs in [5]–[7], [25],

$$\mathbf{J}_k^Z(\mathbf{x}_k, m_k) = \Lambda_k^1(\mathbf{x}_k, m_k) \mathbf{H}_k^T(\mathbf{x}_k) \mathbf{R}_k^{-1}(\mathbf{x}_k) \mathbf{H}_k(\mathbf{x}_k) \quad (50)$$

However, if the TMU is considered to be partially dependent on the T2R geometry, i.e., P_d is state-dependent but \mathbf{R}_k is state-independent parameters when differentiating $\ln p(\mathbf{Z}(k)|\mathbf{x}_k, m_k)$ w.r.t \mathbf{x}_k , \mathbf{C} in (24) becomes zero matrix, the IGF $\Lambda_k^2(\mathbf{x}_k, m_k)$ in (34) coincides to be the additional information impact parameter (AIIP) proposed in [12], and equals to (51).

IV. APPLICATION OF IPCRLB TO RADAR TRAJECTORY CONTROL

The POMDP has been widely used as an online control framework for sensor management, in which the control decision-making problem is formulated as a first-order Markov process over time. Under POMDP, the best control command is selected via optimizing the objective function that quantitatively measures the goodness on the sensor-control resulted estimation. The IPCRLB derived in section III fundamentally formulates the impact of T2R geometry on the radar tracking accuracy and provides a much more accurate MSE bound for radar tracking in clutter with geometry-dependent TMU. To leverage the derived IPCRLB, we propose to formulate the trace of predictive IPCRLB as the objective function and minimize this cost function to select best trajectory-control command to optimize T2R geometry. Compared to the state-of-the-art information-driven and task-driven methods, the proposed approach avoids operating complicated pseudo tracking

using enumerated PIMS, and delivers intensively improved tracking results.

Since the TMU in bistatic radar is more sensitive to the T2R geometry than that in monostatic radar, to better demonstrate trajectory optimization benefits, we concentrate on bistatic radar system with stationary transmitter and control the receiver trajectory to optimize the transmitter-target-receiver geometry. Recall the bistatic radar system depicted in 2D Cartesian coordinate in section II, the full state of receiver consists of 2D position and velocity component, denoted by $\mathbf{x}_{R,k} = [x_{R,k} \ y_{R,k} \ \dot{x}_{R,k} \ \dot{y}_{R,k}]^T = \left[\left(\mathbf{x}_{R,k}^p \right)^T \left(\mathbf{x}_{R,k}^v \right)^T \right]^T$, with the receiver trajectory represented by its position component $\mathbf{x}_{R,k}^p$ over time. In realistic scenario, to guarantee tracking performance, the radar usually operates in a very fast sampling rate, we follow [15]–[18] and assume the receiver moves with a nearly constant velocity (NCV) model during the interval of two consecutive scans, denoted by $T_k = t_k - t_{k-1}$. Therefore, the receiver velocity vector at any time $t_l \in (t_{k-1}, t_k]$ keeps same and equals to the velocity vector at last time t_{k-1} , that is

$$\mathbf{x}_{R,l}^v = \mathbf{x}_{R,k-1}^v = \begin{bmatrix} \dot{x}_{R,k-1} \\ \dot{y}_{R,k-1} \end{bmatrix} = \begin{bmatrix} v_{k-1}^R \cos(w_{k-1}^R) \\ v_{k-1}^R \sin(w_{k-1}^R) \end{bmatrix} \quad (52)$$

where v_{k-1}^R and w_{k-1}^R denote the velocity and heading angle of receiver velocity vector at time t_{k-1} , respectively. Hence, the receiver position at time t_k is collectively determined by its position and velocity at last time t_{k-1} , i.e.,

$$\mathbf{x}_{R,k}^p = \begin{bmatrix} x_{R,k} \\ y_{R,k} \end{bmatrix} = \begin{bmatrix} x_{R,k-1} + v_{k-1}^R T_k \cos(w_{k-1}^R) \\ y_{R,k-1} + v_{k-1}^R T_k \sin(w_{k-1}^R) \end{bmatrix} \quad (53)$$

As shown above, the receiver velocity v_{k-1}^R and heading angle w_{k-1}^R at last time t_{k-1} determine the receiver trajectory position $\mathbf{x}_{R,k}^p$ at current time t_k . Let's define the receiver trajectory control command at t_{k-1} as $\mathbf{u}_{k-1} = [v_{k-1}^R \ w_{k-1}^R]^T$. To highlight the dependence of receiver state at time t_k on the control command at t_{k-1} , we define $\mathbf{x}_{R,k} \triangleq \mathbf{x}_{R,k}(\mathbf{u}_{k-1})$. In consideration of realistic maneuver capability of radar platform, both the value and changing rate of receiver velocity and its heading angle need to satisfy the following constraints

$$\begin{cases} v_{min}^R \leq v_{k-1}^R \leq v_{max}^R, & w_{k-1}^R \leq w_{max}^R \\ v_{k-2}^R - a_{max}^v T_k \leq v_{k-1}^R \leq v_{k-2}^R + a_{max}^v T_k \\ w_{k-2}^R - a_{max}^w T_k \leq w_{k-1}^R \leq w_{k-2}^R + a_{max}^w T_k \end{cases} \quad (54)$$

Note that the receiver platform is usually airborne and needs to keep minimum velocity v_{min}^R to avoid crash, v_{max}^R and w_{max}^R are the maximum velocity and heading angle of receiver platform, a_{max}^v and a_{max}^w are the maximum acceleration and angular rate of receiver platform. $\mathbf{u}_{k-2} = [v_{k-2}^R \ w_{k-2}^R]^T$ denotes the receiver trajectory control command at last time t_{k-2} . (54) indicates \mathbf{u}_{k-1} takes value in a continuous space. For sake of simplicity, we discretize the value space of \mathbf{u}_{k-1} into a finite set of admissible commands, i.e., $\mathbf{U}_{k-1} = \{\mathbf{u}_{k-1}^i\}_{i=1}^{(N_v+1)(N_w+1)}$, with $\mathbf{u}_{k-1}^i = [v_{k-1,i}^R \ w_{k-1,i}^R]^T$ denoting the i -th command. Each element in \mathbf{u}_{k-1}^i needs to satisfy the constraints in (54) and can be calculated by

$$\begin{cases} v_{k-1,i}^R = v_{k-2}^R - a_{max}^v T_k + \zeta_i \frac{2a_{max}^v T_k}{N_v}, & \zeta_i = 0, \dots, N_v \\ w_{k-1,i}^R = w_{k-2}^R - a_{max}^w T_k + \zeta_j \frac{2a_{max}^w T_k}{N_w}, & \zeta_j = 0, \dots, N_w \end{cases} \quad (55)$$

where N_v and N_w are the discretized numbers of receiver velocity and heading angle respectively.

We consider an explicit decision-making problem that selects the best control command \mathbf{u}_{k-1} at time t_{k-1} to obtain proper receiver state $\mathbf{x}_{R,k}(\mathbf{u}_{k-1})$, such that the transmitter-target-receiver geometry at time t_k can be optimized. Based on the designated $\mathbf{x}_{R,k}(\mathbf{u}_{k-1})$, the receiver is actuated accordingly to acquire high-quality target measurement, thereby improving tracking accuracy. The myopic control policy is considered at the rest of this section, the term ‘‘myopic’’ means only deciding one control command one-step ahead rather than planning multiple commands multi-step into the future. To cast the receiver trajectory control problem into the POMDP framework, several other elements need to be defined as follows:

- $p(\mathbf{x}_k|\mathbf{Z}^{k-1})$: predicted density of target state \mathbf{x}_k given measurements up to time t_{k-1}
- \mathbf{U}_{k-1} : a set of finite admissible control commands for radar receiver to operate at time t_{k-1}
- $p(\mathbf{z}_k|\mathbf{x}_k, \mathbf{x}_{R,k}(\mathbf{u}_{k-1}))$: the likelihood of measurement \mathbf{z}_k given target state \mathbf{x}_k and command \mathbf{u}_{k-1} resulted receiver state $\mathbf{x}_{R,k}(\mathbf{u}_{k-1})$ at time t_k
- $C(\mathbf{x}_k, \mathbf{x}_{R,k}(\mathbf{u}_{k-1}))$: a real-valued objective function associated with command \mathbf{u}_{k-1} resulted receiver state $\mathbf{x}_{R,k}(\mathbf{u}_{k-1})$ and target state \mathbf{x}_k

For the objective function, we utilize the trace of predictive IPCRLB as the cost function to measure the MSE error of

trajectory-control resulted target state estimate and find the best control command that minimizes this cost function. At time t_k , the target state \mathbf{x}_k is characterized by its predicted distribution $p(\mathbf{x}_k|\mathbf{Z}^{k-1})$, thus the best command \mathbf{u}_{k-1} is commonly chosen by minimizing the statistical mean of the cost function $C(\mathbf{x}_k, \mathbf{x}_{R,k}(\mathbf{u}_{k-1}))$ over all realizations of \mathbf{x}_k , hence, we can formulate the receiver trajectory control problem as

$$\begin{aligned} \mathbf{u}_{k-1} &= \min_{\mathbf{u}_{k-1}^i \in \mathbf{U}_{k-1}} E_{\mathbf{x}_k} \{C(\mathbf{x}_k, \mathbf{x}_{R,k}(\mathbf{u}_{k-1}^i))\} \\ &= \min_{\mathbf{u}_{k-1}^i \in \mathbf{U}_{k-1}} Tr(\mathbf{J}_k^{-1})_{\mathbf{x}_k = \hat{\mathbf{x}}_k|_{k-1}} \end{aligned} \quad (56)$$

with elements of each command \mathbf{u}_{k-1}^i constrained by (54).

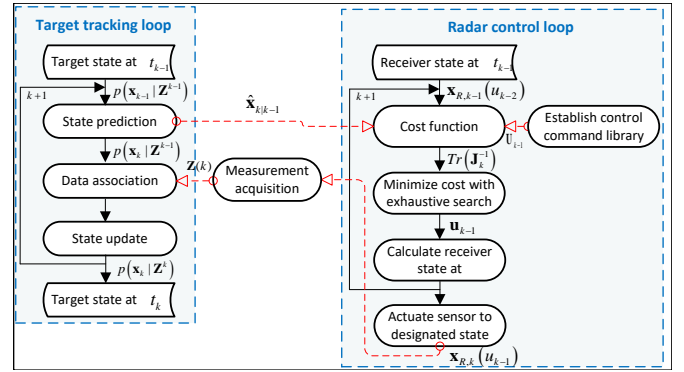


Fig. 3. Receiver trajectory control framework

The receiver trajectory control framework is shown in Fig. 3, in which the interaction between trajectory control loop and target tracking loop is clearly demonstrated. Based upon the outputs at time t_{k-1} from tracking loop (target state estimate $p(\mathbf{x}_{k-1}|\mathbf{Z}^{k-1})$) and control loop (receiver state $\mathbf{x}_{R,k-1}(\mathbf{u}_{k-2})$), main steps of receiver trajectory control are summarized as follows:

- step 1: propagate $p(\mathbf{x}_{k-1}|\mathbf{Z}^{k-1})$ through target dynamic model to obtain predicted state estimate $p(\mathbf{x}_k|\mathbf{Z}^{k-1})$ at time t_k . Note that the target tracking considered in this paper assumes target track has been successfully initiated and concentrates on the track maintenance by implementing data association and filtering update to obtain target posterior state estimate at each time.
- step 2: based upon receiver state $\mathbf{x}_{R,k-1}(\mathbf{u}_{k-2})$, generate each admissible command via (55) and establish the discretized receiver trajectory control command library $\mathbf{U}_{k-1} = \{\mathbf{u}_{k-1}^i\}_{i=1}^{(N_v+1)(N_w+1)}$, with each element of \mathbf{u}_{k-1}^i satisfied the platform maneuver constraints shown in (54),
- step 3: calculate the cost function $Tr(\mathbf{J}_k^{-1})_{\mathbf{x}_k = \hat{\mathbf{x}}_k|_{k-1}}$ that evaluates at the mean of predicted state estimate $p(\mathbf{x}_k|\mathbf{Z}^{k-1})$.
- step 4: select the best control command \mathbf{u}_{k-1} that minimizes $Tr(\mathbf{J}_k^{-1})_{\mathbf{x}_k = \hat{\mathbf{x}}_k|_{k-1}}$ using exhaustive search inside the discrete control command space \mathbf{U}_{k-1} .
- step 5: based on the selected command \mathbf{u}_{k-1} , calculate the full state of receiver $\mathbf{x}_{R,k}(\mathbf{u}_{k-1})$ by (52) and (53).

- step 6: actuate receiver to the designated state $\mathbf{x}_{R,k}(\mathbf{u}_{k-1})$ to acquire high quality radar measurements $\mathbf{Z}(k)$ at time t_k , then fed $\mathbf{Z}(k)$ back to the target tracking loop to implement data association and state update to calculate the posterior estimate $p(\mathbf{x}_k|\mathbf{Z}^k)$ at time t_k .

V. SIMULATION AND DISCUSSION

In this section, we consider a scenario deploying a bistatic radar to track a moving target in clutter in 2D surveillance space. The advanced television systems committee (ATSC) signal is selected as the illuminated signal, the FIM for time delay and Doppler shift of ATSC signal is then given by [27]

$$\mathbf{J}_{ATSC}(\tau_k, \xi_k) = \Psi(\Delta_k) \times \begin{bmatrix} \frac{2\alpha^2}{T_{Sym}^2} \left(\frac{-1}{\pi^2} + \frac{1}{96\alpha^2} + \frac{1}{8} \right) & 0 \\ 0 & 2T_{Sym}^2 \left(\frac{1}{4\alpha} + \frac{N^2-1}{3} \right) \end{bmatrix} \quad (57)$$

where T_{Sym} is the symbol period of the ATSC signal, α is the roll-off factor, and N is the number of transmitted symbols. By substituting the diagonal elements of matrix at the right hand side of (57) to (14), the full expressions of $\mathbf{R}_k(\Delta_k)$ can be obtained. Following [27], we set $\alpha = 0.05762$, $T_{Sym} = 93ns$, $N = 1076000$, $f_c = 63.1MHz$, $\sigma_{\theta_0} = 3^\circ$. Remainder of this section conducts three case studies to validate the effectiveness and superiority of model and methods proposed at section II, III and IV, respectively.

A. Case 1: impact of T2R geometry on target measurement uncertainty

This case study aims to investigate the impact of T2R geometry Δ_k on P_d and \mathbf{R}_k via (6) and (14) proposed in section II. Since the location and shape of triangle Δ_k are uniquely described by $(d_k, L_k, \theta_k, \theta_{TR,k})$, to obtain diverse T2R geometries, we set both the transmitter and receiver to be static with $L_k = 5km$ and $\theta_{RT,k} = \pi$, and control target moving to generate different target range $R_{R,k}$ or DOA θ_k . The target velocity is set to be a constant $50m/s$, bistatic angle β_k equals to 45° , the false alarm rate and transmitted signal constant are set to be $P_{FA} = 0.001$ and $\vartheta_0 = 5000$, respectively.

As shown in Fig. 4, the TMU in terms of measurement error standard deviation $\sigma_d, \sigma_v, \sigma_\theta$ and detection probability P_d varies evidently as the DOA θ_k changes from 0° to 360° w.r.t. different target range $R_{R,k}$. At $\theta_k = 180^\circ$, σ_d, σ_v and σ_θ reach their minimums while P_d reaches its maximum, both indicating the least TMU. This is because when $\theta_k = 180^\circ$, the transmitter, target and receiver are collinear, the value of $R_{T,k}R_{R,k}$ in (7) decreases to the minimum such that the echo SNR Ψ is maximized. Notably, σ_v slightly increases near $\theta_k = 180^\circ$ due to the resolution loss in Doppler blind zone. Fig. 5 shows that the TMU changes dramatically with varied target range $R_{R,k}$ w.r.t. different target DOA θ_k . It can be observed there that target measurement achieves the least uncertainty when target moves towards the transmitter-receiver baseline. Therefore, these numerical results validate the TMU in terms of both measurement error covariance and detection probability is indeed highly dependent on the T2R geometry.

B. Case 2: comparison of IPCRLB with state-of-the-art bounds

To validate the superiority of the proposed IPCRLB for radar tracking in clutter with geometry-dependent TMU, two state-of-the-art bounds are implemented and compared. They are the conventional PCRLB [5]–[7], [25] and the EFIM [12], respectively. To investigate the impact of T2R geometry on the compared bounds, following the same setting as case 1, the target is controlled to move along its trajectory with varying DOA θ_k or range $R_{R,k}$ to generate different T2R geometries.

Comparisons of the trace of three bounds versus varied θ_k and $R_{R,k}$ are demonstrated in Fig. 6 and 7 respectively. As shown there, the proposed IPCRLB delivers the lowest MSE bound, followed by the EFIM, with conventional PCRLB the highest bound. This is because IPCRLB extracts more additional target Fisher information by fully considering both P_d and \mathbf{R}_k as state-dependent parameters when differentiating $\ln p(\mathbf{Z}(k)|\mathbf{x}_k, m_k)$ w.r.t \mathbf{x}_k . In contrast, EFIM ignores the dependence of \mathbf{R}_k on T2R geometry and PCRLB completely treats TMU as state-independent parameters, leading to increased (over-conservative) MSE bound. Furthermore, as shown in Fig. 6a, Fig. 6b and Fig.7, the improvement of IPCRLB over PCRLB and EFIM increases as TMU rises (i.e., σ_d, σ_v and σ_θ increase while P_d decreases as shown in Fig. 4 and Fig. 5). However, if TMU is too high, the improvement of IPCRLB over EFIM vanishes as indicated in Fig. 6c and Fig. 6d. Moreover, similarly improved results of proposed IPCRLB over compared bound w.r.t. varied false alarm rate and transmitted signal constant can be observed in Fig.8a and Fig.8b, respectively. In consequence, numerical results of this case study verify the superiority of proposed IPCRLB compared to state-of-the-art bounds.

C. Case 3: superiority of IPCRLB applied to receiver trajectory control

To validate the superiority of proposed IPCRLB formulating MSE lower bound for radar tracking in clutter with geometry-dependent TMU, the trace of predictive IPCRLB is utilized as the cost function and minimized to optimize the T2R geometry to acquire high-quality target measurement for improved radar tracking in clutter. For simplicity, this control method is abbreviated as $\min \text{tr}(\text{IPCRLB})$. Several state-of-the-art radar trajectory control methods are also implemented and compared:

- max KLD: a representative information-driven method, the Kullback-Leibler divergence(KLD) is formulated as a reward function and maximized to select the best receiver moving control command [15].
- min PDST: a representative task-driven method, the posterior distance between sensor and target(PDST) is formulated as a cost function and minimized to select the best receiver moving control command [24].
- $\min \text{tr}(\text{PCRLB})$: bound based method, the trace of predictive PCRLB is utilized as the cost function and minimized to select the best receiver moving control command.
- fixed: the receiver keeps fixed at its original position.

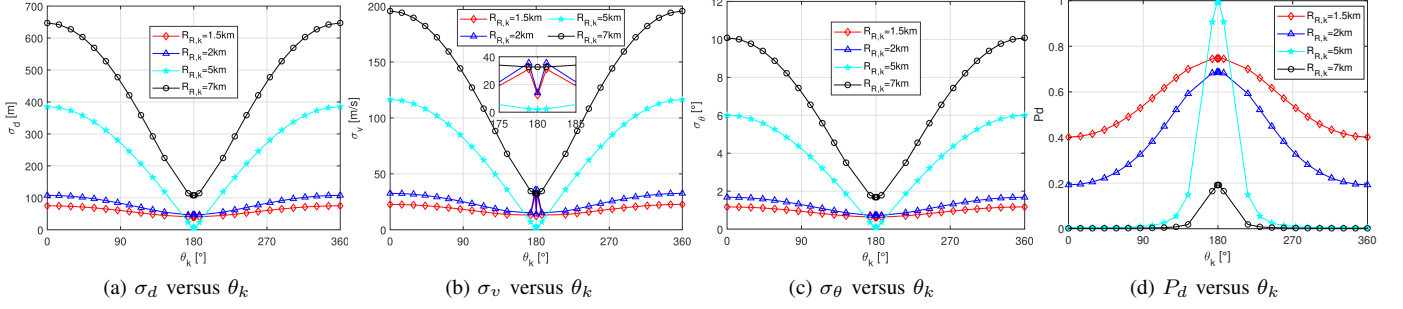


Fig. 4. TMU varies as target DOA θ_k w.r.t. different target range $R_{R,k}$.

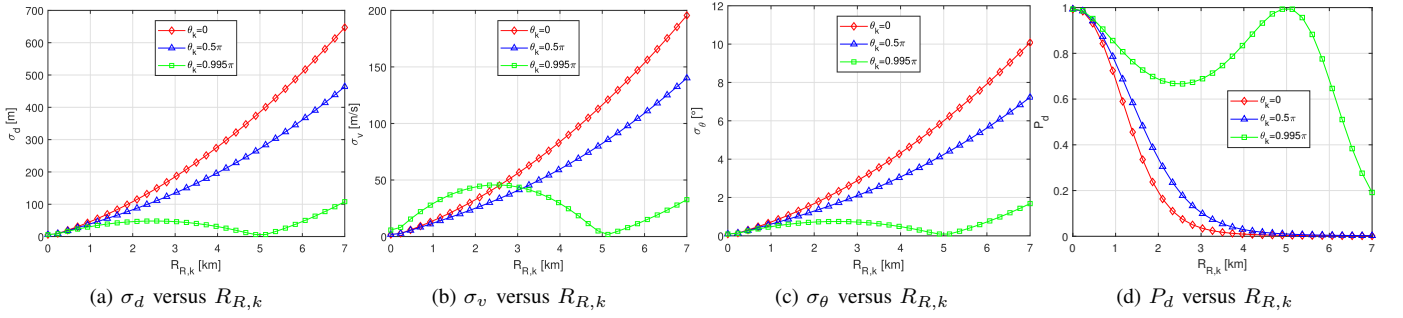


Fig. 5. TMU varies as target range $R_{R,k}$ w.r.t. different target DOA θ_k .

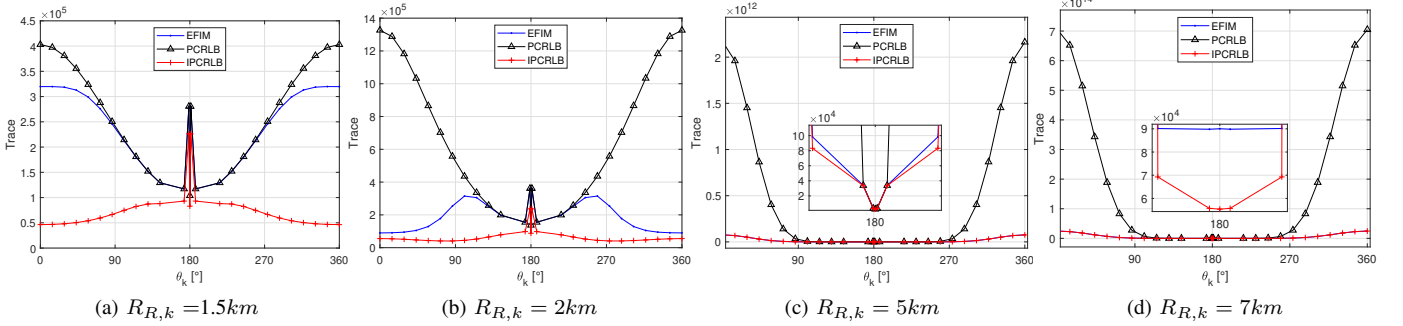


Fig. 6. Comparison of the trace of different bounds versus varied target DOA θ_k .

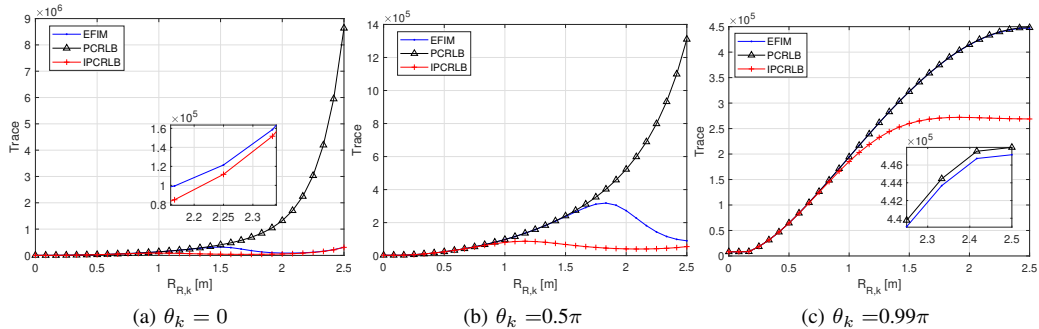


Fig. 7. Comparison of trace of different bounds versus varied target range $R_{R,k}$.

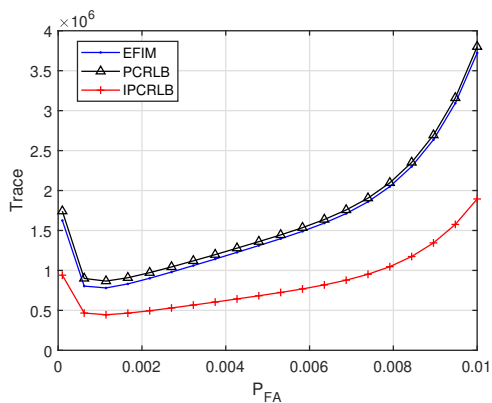
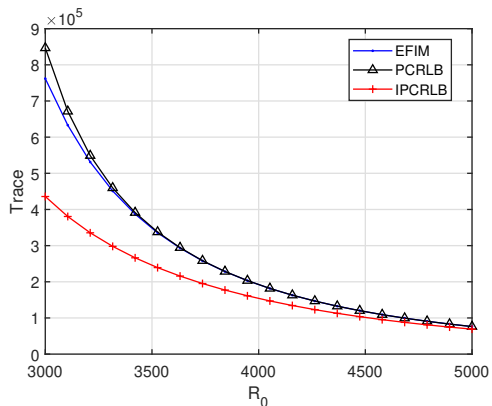
(a) Trace of compared PCRLBs versus P_{FA} (b) Trace of compared PCRLBs versus ϑ_0

Fig. 8. Comparison of trace of different bounds versus varied false alarm rate and transmitted signal constant

- random: randomly choose the command to control receiver moving trajectory.

Transmitter is fixed at the origin, initial state of receiver equals $\mathbf{x}_{R,0} = [5000m \ 0m \ 0m/s \ 0m/s]^T$, the target moves with a nearly constant velocity model with initial state $\mathbf{x}_0 = [5000m \ 5000m \ -80m/s \ -100m/s]^T$, the minimum and maximum velocity of receiver platform are set to be $v_{min}^R = 1m/s$ and $v_{max}^R = 100m/s$, the maximum acceleration and angular rate of receiver platform are set to be $a_{max}^v = 5m/s^2$ and $a_{max}^w = 30^\circ/s^2$, discretized numbers of receiver platform velocity and heading angle are set to be $N_v = 40$ and $N_w = 20$. ϑ_0 is set to be 9000, the experiment repeats for 200 Monte Carlo runs. Other parameters are set the same as case 1.

The T2R geometries of different receiver trajectory control methods are shown in Fig.9. Except for the fixed and random methods, all others control the receiver moving towards the target but with different trajectories. Fig.10 demonstrates the means and standard deviations of σ_d , σ_v , σ_θ and P_d at each time among compared control methods, and the min tr(IPCRLB) delivers least TMU. After operating target tracking based upon acquired measurements, the RMSEs of position and velocity are given in Fig.11 and Fig.12. Among compared control methods, since the min tr(IPCRLB) delivers least TMU, it provides the most accurate estimation of target po-

sition and velocity, followed by min tr(PCRLB), min (PDST) and max (KLD). The fixed and random methods perform the worst. Since IPCRLB fully accounts for the impact of T2R geometry on the TMU and eventual MSE lower bound, it formulates the bound more accurately than PCRLB for radar tracking in clutter, hence, the min tr(IPCRLB) tends to optimize the T2R geometry more effectively than the min tr(PCRLB). Unlike the two bound-based control methods that optimize the T2R geometry to straightforwardly minimize theoretical tracking error, the min (PDST) minimizes the target-to-receiver distance and the max (KLD) maximizes information gain to control the receiver trajectory. Therefore, both min (PDST) and max (KLD) belong to indirect T2R geometry optimization, which inevitably results in degraded optimization benefits.

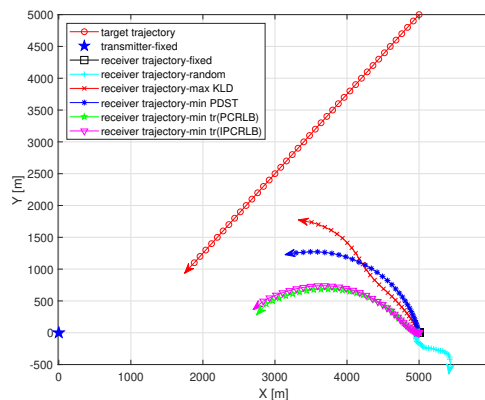


Fig. 9. Comparison of T2R Geometries of different receiver trajectory control methods.

VI. CONCLUSION

This paper investigates radar tracking in clutter with T2R geometry-dependent TMU. First of all, the target measurement error covariance is formulated as a function of transmitted signal, target and radar state, and its generalized form is then approximated to specify the impact of T2R geometry on error covariance. Based on the approximated uncertainty model, an improved PCRLB (IPCRLB) is rigorously derived for radar tracking in clutter by fully accounting for radar measurement uncertainty in terms of both MOU and geometry-dependent TMU. The derived IPCRLB is then applied to radar trajectory control to effectively optimize the T2R geometry, thereby acquiring high-quality target measurement for improved tracking accuracy. Numerical results validate that the new bound is more accurate than existing PCRLBs and provides an effective tool for sensor resource management.

APPENDIX A

DERIVATION OF δ_k AND $\cos\left(\frac{\beta_k}{2}\right)$

By a canonical definition [29], the Doppler shift ξ_k ignoring relativistic effects, is the time rate of change of bistatic range normalized by the wavelength $\frac{c}{f_c}$, i.e.,

$$\xi_k = \frac{f_c}{c} \left(\frac{dR_{T,k}}{dt} + \frac{dR_{R,k}}{dt} \right) \quad (\text{A-1})$$

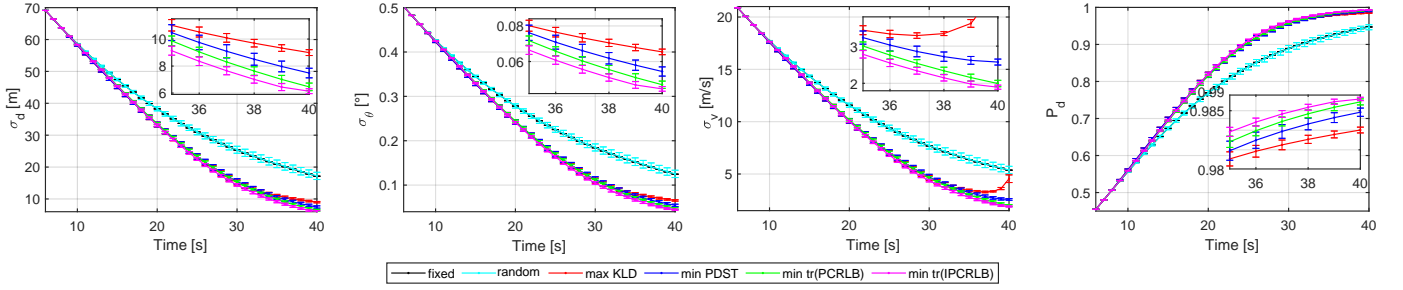


Fig. 10. Comparison of target measurement uncertainties among different receiver trajectory control methods.

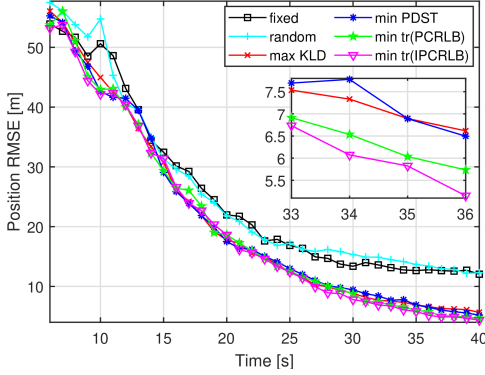


Fig. 11. Comparison of position RMSEs among different receiver trajectory control methods.

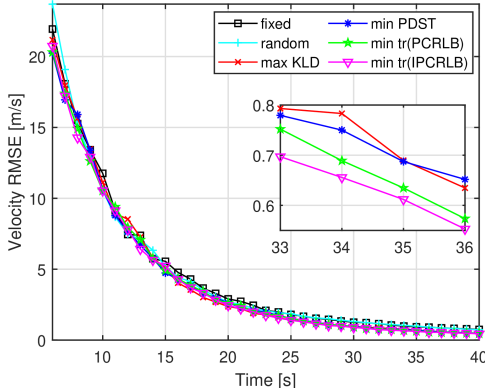


Fig. 12. Comparison of velocity RMSEs among different receiver trajectory control methods.

When the target is moving (i.e., $\|\mathbf{x}_k^v\|_2 \neq 0$) and the transmitter and receiver are stationary ($\|\mathbf{x}_{T,k}^v\|_2 = \|\mathbf{x}_{R,k}^v\|_2 = 0$), the Doppler shift at the receiver due to the target motion is the sum of the projection of target velocity vector onto the transmitter-to-target line-of-sight (LOS) and the receiver-to-target LOS, normalized by the wavelength, given by

$$\begin{aligned} \xi_{Tgt,k} &= \frac{f_c}{c} \left(\|\mathbf{x}_k^v\|_2 \cos\left(\delta_k - \frac{\beta_k}{2}\right) + \|\mathbf{x}_k^v\|_2 \cos\left(\delta_k + \frac{\beta_k}{2}\right) \right) \\ &= \frac{2f_c}{c} \|\mathbf{x}_k^v\|_2 \cos(\delta_k) \cos\left(\frac{\beta_k}{2}\right) \end{aligned} \quad (\text{A-2})$$

As shown in Fig.1, δ_k is the aspect angle of target velocity vector \mathbf{x}_k^v referenced to the bistatic bisector, measured positive clockwise from the bistatic bisector. When the target is stationary ($\|\mathbf{x}_k^v\|_2 = 0$) and the transmitter and receiver are moving ($\|\mathbf{x}_{T,k}^v\|_2 = \|\mathbf{x}_{R,k}^v\|_2 \neq 0$), the Doppler shift at the receiver due to the combined transmitter and receiver motion is the sum of the projection of transmitter velocity vector onto transmitter-to-target LOS and receiver velocity vector onto receiver-to-target LOS, given by

$$\begin{aligned} \xi_{TR,k} &= \frac{f_c}{c} \left(\|\mathbf{x}_{T,k}^v\|_2 \cos(\delta_{T,k} - \theta_{T,k}) + \|\mathbf{x}_{R,k}^v\|_2 \cos(\delta_{R,k} - \theta_k) \right) \end{aligned} \quad (\text{A-3})$$

where $\delta_{T,k}$ and $\delta_{R,k}$ are the aspect angles of transmitter velocity vector and receiver velocity vector referenced to the x -axis respectively, which are measured positive counter-clockwise from the x -axis. When the target, transmitter and receiver are all moving, the Doppler shift at the receiver due to all sites motion is the sum of (A-2) and (A-3), thus

$$\begin{aligned} \xi_k &= \frac{f_c}{c} \left(2\|\mathbf{x}_k^v\|_2 \cos\delta_k \cos\left(\frac{\beta_k}{2}\right) \right. \\ &\quad \left. + \|\mathbf{x}_{T,k}^v\|_2 \cos(\delta_{T,k} - \theta_{T,k}) + \|\mathbf{x}_{R,k}^v\|_2 \cos(\delta_{R,k} - \theta_k) \right) \end{aligned} \quad (\text{A-4})$$

with the law of cosine, we have

$$\begin{aligned} \cos\left(\frac{\beta_k}{2}\right) &= \sqrt{\frac{1 + \cos\beta_k}{2}} \\ &= \sqrt{\frac{1}{2} + \frac{1}{2} \frac{R_{T,k}^2 + R_{R,k}^2 - L_k^2}{2R_{T,k}R_{R,k}}} \end{aligned} \quad (\text{A-5})$$

As seen above, the Doppler shift ξ_k implicitly relates to the bistatic range d_k through the term $\cos\left(\frac{\beta_k}{2}\right)$, with $d_k = R_{T,k} + R_{R,k}$. Again, applying the law of cosines to the T2R triangle depicted in Fig.1, with some mathematical transformations, we have

$$\begin{aligned} R_{R,k} &= \frac{d_k^2 - L_k^2}{2(d_k + L_k \cos(\theta_k - \theta_{TR,k}))} \\ R_{T,k} &= \frac{d_k^2 + L_k^2 + 2d_k L_k \cos(\theta_k - \theta_{TR,k})}{2(d_k + L_k \cos(\theta_k - \theta_{TR,k}))} \end{aligned} \quad (\text{A-6})$$

By substituting (A-6) to (A-5), $\cos\left(\frac{\beta_k}{2}\right)$ can be explicitly expressed as a function of d_k as shown in (5). Then by substituting (5) to (A-4), the mathematical relationship between ξ_k and d_k can be finally obtained as (4).

$$\begin{aligned} \mathbb{E}_{\tilde{\mathbf{Z}}(k)} \{\Gamma_{\mathbf{BB}^T}\} &= \frac{\lambda^2 V_g^2 m_k^2 (P_{FA}^g)^{2/(1+\Psi_k(\mathbf{x}_k))}}{\ell_g^4} \frac{\ln^2 P_{FA}^g}{[1 + \Psi_k(\mathbf{x}_k)]^4} \\ &\times \int_{\tilde{\mathbf{z}}_k^1 \in \hat{\Xi}} \cdots \int_{\tilde{\mathbf{z}}_k^{m_k} \in \hat{\Xi}} \frac{1}{p(\tilde{\mathbf{Z}}(k) | \mathbf{x}_k, m_k)} \underbrace{\left[\frac{\sum_{i=1}^{m_k} \sum_{j=1}^{m_k} p(\tilde{\mathbf{z}}_k^i) p(\tilde{\mathbf{z}}_k^j)}{m_k^2 V_g^{2m_k-2}} - \frac{2 \sum_{i=1}^{m_k} p(\tilde{\mathbf{z}}_k^i)}{m_k V_g^{2m_k-1}} + \frac{1}{V_g^{2m_k}} \right]}_{\Omega_1} d\tilde{\mathbf{z}}_k^1 \cdots d\tilde{\mathbf{z}}_k^{m_k} \end{aligned} \quad (\text{B-2})$$

$$\begin{aligned} \mathbb{E}_{\tilde{\mathbf{Z}}(k)} \{\Gamma_{\mathbf{BC}^T}\} &= \frac{d_g(\mathbf{x}_k, m_k)}{\Psi_k(\mathbf{x}_k) V_g^{m_k-2}} \frac{\ln P_{FA}^g}{[1 + \Psi_k(\mathbf{x}_k)]^2} \frac{\lambda (P_{FA}^g)^{1/(1+\Psi_k(\mathbf{x}_k))}}{\ell_g^2} \\ &\times \int_{\tilde{\mathbf{z}}_k^1 \in \hat{\Xi}} \cdots \int_{\tilde{\mathbf{z}}_k^{m_k} \in \hat{\Xi}} \frac{1}{p(\tilde{\mathbf{Z}}(k) | \mathbf{x}_k, m_k)} \underbrace{\left[\frac{\sum_{i=1}^{m_k} \sum_{j=1}^{m_k} p(\tilde{\mathbf{z}}_k^i) p(\tilde{\mathbf{z}}_k^j) [\tilde{\gamma}(\tilde{\mathbf{z}}_k^j) - n]}{m_k V_g^{m_k-1}} - \frac{\sum_{i=1}^{m_k} p(\tilde{\mathbf{z}}_k^i) [\tilde{\gamma}(\tilde{\mathbf{z}}_k^i) - n]}{V_g^{m_k}} \right]}_{\Omega_2} d\tilde{\mathbf{z}}_k^1 \cdots d\tilde{\mathbf{z}}_k^{m_k} \end{aligned} \quad (\text{B-3})$$

$$\begin{aligned} \mathbb{E}_{\tilde{\mathbf{Z}}(k)} \{\Gamma_{\mathbf{CC}^T}\} &= \frac{d_g^2(\mathbf{x}_k, m_k)}{4\Psi_k^2(\mathbf{x}_k) m_k^2 V_g^{2m_k-2}} \int_{\tilde{\mathbf{z}}_k^1 \in \hat{\Xi}} \cdots \int_{\tilde{\mathbf{z}}_k^{m_k} \in \hat{\Xi}} \frac{1}{p(\tilde{\mathbf{Z}}(k) | \mathbf{x}_k, m_k)} \underbrace{\sum_{i=1}^{m_k} \sum_{j=1}^{m_k} p(\tilde{\mathbf{z}}_k^i) [\tilde{\gamma}(\tilde{\mathbf{z}}_k^i) - n] p(\tilde{\mathbf{z}}_k^j) [\tilde{\gamma}(\tilde{\mathbf{z}}_k^j) - n]}_{\Omega_3} d\tilde{\mathbf{z}}_k^1 \cdots d\tilde{\mathbf{z}}_k^{m_k} \end{aligned} \quad (\text{B-4})$$

APPENDIX B

DERIVATION OF $\Lambda_k^2(\mathbf{x}_k, m_k)$

With the changed variable $\tilde{\mathbf{z}}_k^i$ defined in (40) and its corresponding integral region presented in (41), (36) can be rearranged as

$$\begin{aligned} \Lambda_k^2(\mathbf{x}_k, m_k) &= \mathbb{E}_{\tilde{\mathbf{Z}}(k)} \{\Gamma_{\mathbf{BB}^T}\} + \mathbb{E}_{\tilde{\mathbf{Z}}(k)} \{\Gamma_{\mathbf{BC}^T}\} + \mathbb{E}_{\tilde{\mathbf{Z}}(k)} \{\Gamma_{\mathbf{CC}^T}\} \end{aligned} \quad (\text{B-1})$$

with each expectation terms above given by (B-2), (B-3), (B-4), let define

$$\ell_g = [1 - P_d^g(\mathbf{x}_k)] \lambda V_g + m_k P_d^g(\mathbf{x}_k) \quad (\text{B-5})$$

and

$$\tilde{\gamma}(\tilde{\mathbf{z}}_k^i) = (\tilde{\mathbf{z}}_k^i)^T \mathbf{R}_k^{-1}(\mathbf{x}_k) \tilde{\mathbf{z}}_k^i \quad (\text{B-6})$$

It is easy to see from (B-2) that the integral of $p(\tilde{\mathbf{z}}_k^i) p(\tilde{\mathbf{z}}_k^j)$ is all equal in value for $i = 1, \dots, m_k, j = 1, \dots, m_k$, and the integral of $p(\tilde{\mathbf{z}}_k^i)$ is also all equal in value for $i = 1, \dots, m_k$, therefore, by removing the summation notations inside the integral function of (B-2), Ω_1 reduces to

$$\begin{aligned} \Omega_1 &= \frac{e^{-\tilde{\gamma}(\tilde{\mathbf{z}}_k^1)} + (m_k - 1) e^{-\frac{\tilde{\gamma}(\tilde{\mathbf{z}}_k^1) + \tilde{\gamma}(\tilde{\mathbf{z}}_k^2)}{2}}}{m_k V_g^{2m_k-2} (2\pi)^n |\mathbf{R}_k(\mathbf{x}_k)|} \\ &\quad - \frac{2e^{-\frac{\tilde{\gamma}(\tilde{\mathbf{z}}_k^1)}{2}}}{V_g^{2m_k-1} \sqrt{(2\pi)^n |\mathbf{R}_k(\mathbf{x}_k)|}} + \frac{1}{V_g^{2m_k}} \end{aligned} \quad (\text{B-7})$$

Similarly, by removing the summation notations inside the integral function of (B-3) and (B-4), we have

$$\begin{aligned} \Omega_2 &= -\frac{m_k e^{-\frac{\tilde{\gamma}(\tilde{\mathbf{z}}_k^1)}{2}} [\tilde{\gamma}(\tilde{\mathbf{z}}_k^1) - n]}{V_g^{m_k} \sqrt{(2\pi)^n |\mathbf{R}_k(\mathbf{x}_k)|}} + \\ &\quad \frac{e^{-\tilde{\gamma}(\tilde{\mathbf{z}}_k^1)} [\tilde{\gamma}(\tilde{\mathbf{z}}_k^1) - n] + (m_k - 1) e^{-\frac{\tilde{\gamma}(\tilde{\mathbf{z}}_k^1) + \tilde{\gamma}(\tilde{\mathbf{z}}_k^2)}{2}} [\tilde{\gamma}(\tilde{\mathbf{z}}_k^2) - n]}{V_g^{m_k-1} (2\pi)^n |\mathbf{R}_k(\mathbf{x}_k)|} \end{aligned} \quad (\text{B-8})$$

$$\begin{aligned} \Omega_3 &= \frac{m_k e^{-\tilde{\gamma}(\tilde{\mathbf{z}}_k^1)} [\tilde{\gamma}(\tilde{\mathbf{z}}_k^1) - n]^2}{(2\pi)^n |\mathbf{R}_k(\mathbf{x}_k)|} + \\ &\quad \frac{m_k (m_k - 1) e^{-\frac{\tilde{\gamma}(\tilde{\mathbf{z}}_k^1) + \tilde{\gamma}(\tilde{\mathbf{z}}_k^2)}{2}} [\tilde{\gamma}(\tilde{\mathbf{z}}_k^1) - n] [\tilde{\gamma}(\tilde{\mathbf{z}}_k^2) - n]}{(2\pi)^n |\mathbf{R}_k(\mathbf{x}_k)|} \end{aligned} \quad (\text{B-9})$$

To further simplify the integral functions above, again make the change of variable

$$\hat{\mathbf{z}}_k^i[h] = \frac{\tilde{\mathbf{z}}_k^i[h]}{\sigma_h}, h = 1, \dots, n \quad (\text{B-10})$$

let $\hat{\mathbf{z}}_k^i = [\hat{\mathbf{z}}_k^i[1] \cdots \hat{\mathbf{z}}_k^i[n]]^T, i = 1, \dots, m_k$, the integral region of $\hat{\mathbf{z}}_k^i$ then converts to $\tilde{\Xi} = [-g, g] \times \cdots \times [-g, g]$, hence we have the following differentiating relationship

$$d\tilde{\mathbf{z}}_k^1 \cdots d\tilde{\mathbf{z}}_k^{m_k} = |\mathbf{R}_k(\mathbf{x}_k)|^{m_k/2} d\hat{\mathbf{z}}_k^1 \cdots d\hat{\mathbf{z}}_k^{m_k} \quad (\text{B-11})$$

and $\tilde{\gamma}(\tilde{\mathbf{z}}_k^i)$ in (B-6) can be simplified as

$$\tilde{\gamma}(\tilde{\mathbf{z}}_k^i) = \sum_{h=1}^n (\tilde{\mathbf{z}}_k^i[h])^2 \quad (\text{B-11})$$

Substituting (B-11) to (B-7), (B-8), (B-9), their results together with (B-11) are then substituted to (B-2)-(B-4), the final form of (B-1) can be obtained as in (43)-(46).

REFERENCES

- [1] L. Harry, V. TREES, DETECTION, ESTIMATION, AND MODULATION THEORY. PT. 01. DETECTION, ESTIMATION, AND LINEAR MODULATION THEORY., JOHN WILEY., 1968.
- [2] P. Tichavsky, C. H. Muravchik, A. Nehorai, Posterior cramer-rao bounds for discrete-time nonlinear filtering, *IEEE Transactions on signal processing* 46 (5) (1998) 1386–1396.
- [3] T. Kirubarajan, Y. Bar-Shalom, Low observable target motion analysis using amplitude information, *IEEE Transactions on Aerospace and Electronic Systems* 32 (4) (1996) 1367–1384.
- [4] R. Niu, P. Willett, Y. Bar-Shalom, Matrix crlb scaling due to measurements of uncertain origin, *IEEE Transactions on Signal Processing* 49 (7) (2001) 1325–1335.
- [5] M. Hernandez, A. Marrs, N. Gordon, S. Maskell, C. Reed, Cramer-rao bounds for non-linear filtering with measurement origin uncertainty, in: *Proceedings of the Fifth International Conference on Information Fusion. FUSION 2002*, (IEEE Cat. No. 02EX5997), Vol. 1, IEEE, 2002, pp. 18–25.
- [6] X. Zhang, P. Willett, Cramer-rao bounds for discrete time linear filtering with measurement origin uncertainty, in: *Proceedings of the Workshop on Estimation, Tracking and Fusion: A Tribute to Yaakov Bar-Shalom*, 2001, pp. 546–561.
- [7] M. L. Hernandez, A. Farina, B. Ristic, Pcrbl for tracking in cluttered environments: Measurement sequence conditioning approach, *IEEE Transactions on Aerospace and Electronic systems* 42 (2) (2006) 680–704.
- [8] M. Hernandez, T. Kirubarajan, Y. Bar-Shalom, Multisensor resource deployment using posterior cramer-rao bounds, *IEEE Transactions on Aerospace and Electronic Systems* 40 (2) (2004) 399–416.
- [9] B. Ristic, A. Farina, M. Hernandez, Cramer-rao lower bound for tracking multiple targets, *IEE Proceedings-Radar, Sonar and Navigation* 151 (3) (2004) 129–134.
- [10] R. Tharmarasa, T. Kirubarajan, M. L. Hernandez, A. Sinha, Pcrbl-based multisensor array management for multitarget tracking, *IEEE Transactions on Aerospace and Electronic Systems* 43 (2) (2007) 539–555.
- [11] X. Song, P. Willett, S. Zhou, On fisher information reduction for range-only localization with imperfect detection, *IEEE Transactions on Aerospace and Electronic Systems* 48 (4) (2012) 3694–3702.
- [12] J. Yan, H. Liu, W. Pu, Z. Bao, Exact fisher information matrix with state-dependent probability of detection, *IEEE Transactions on Aerospace and Electronic Systems* 53 (3) (2017) 1555–1561.
- [13] A. N. Bishop, B. Fidan, B. D. Anderson, K. Doğançay, P. N. Pathirana, Optimality analysis of sensor-target localization geometries, *Automatica* 46 (3) (2010) 479–492.
- [14] N. H. Nguyen, K. Doğançay, Signal processing for multistatic radar systems: Adaptive waveform selection, *Optimal Geometries and Pseudolinear Tracking Algorithms*, Academic Press, 2019.
- [15] R. P. Mahler, Global posterior densities for sensor management, in: *Acquisition, tracking, and pointing XII*, Vol. 3365, SPIE, 1998, pp. 252–263.
- [16] Sensor management for multi-target tracking via multi-bernoulli filtering, *Automatica* 50 (4) (2014) 1135–1142.
- [17] M. Beard, B.-T. Vo, B.-N. Vo, S. Arulampalam, Void probabilities and cauchy-schwarz divergence for generalized labeled multi-bernoulli models, *IEEE Transactions on Signal Processing* 65 (19) (2017) 5047–5061.
- [18] W. Wu, H. Sun, Y. Cai, J. Xiong, Mm-gmb filter-based sensor control for tracking multiple maneuvering targets hidden in the doppler blind zone, *IEEE Transactions on Signal Processing* 68 (2020) 4555–4567.
- [19] M. Kalandros, Covariance control for multisensor systems, *IEEE Transactions on Aerospace and Electronic Systems* 38 (4) (2002) 1138–1157.
- [20] C. Yang, L. Kaplan, E. Blasch, Performance measures of covariance and information matrices in resource management for target state estimation, *IEEE Transactions on Aerospace and Electronic Systems* 48 (3) (2012) 2594–2613.
- [21] A. K. Gostar, R. Hoseinnezhad, A. Bab-Hadiashar, Multi-bernoulli sensor control via minimization of expected estimation errors, *IEEE Transactions on Aerospace and Electronic Systems* 51 (3) (2015) 1762–1773.
- [22] X. Wang, R. Hoseinnezhad, A. K. Gostar, T. Rathnayake, B. Xu, A. Bab-Hadiashar, Multi-sensor control for multi-object bayes filters, *Signal Processing* 142 (2018) 260–270.
- [23] A. K. Gostar, R. Hoseinnezhad, A. Bab-Hadiashar, W. Liu, Sensor-management for multitarget filters via minimization of posterior dispersion, *IEEE Transactions on Aerospace and Electronic Systems* 53 (6) (2017) 2877–2884.
- [24] W. Li, C. Han, Dual sensor control scheme for multi-target tracking, *Sensors* 18 (5) (2018).
- [25] P. Stinco, M. S. Greco, F. Gini, A. Farina, Posterior cramer-rao lower bounds for passive bistatic radar tracking with uncertain target measurements, *Signal Processing* 93 (12) (2013) 3528–3540.
- [26] M. A. Alslaimy, R. J. Burkholder, G. E. Smith, Measurements accuracy evaluation for atsc signal-based passive radar systems, *IEEE Transactions on Aerospace and Electronic Systems* 57 (4) (2021) 2514–2525.
- [27] M. Alslaimy, G. E. Smith, Atsc signal cramer-rao lower bound for emitter selection in passive radar systems, in: *2019 IEEE Radar Conference (RadarConf)*, IEEE, 2019, pp. 1–6.
- [28] T. Tsao, M. Slamani, P. Varshney, D. Weiner, H. Schwarzlander, S. Borek, Ambiguity function for a bistatic radar, *IEEE Transactions on Aerospace and Electronic Systems* 33 (3) (1997) 1041–1051.
- [29] N. J. Willis, *Bistatic radar*, Vol. 2, SciTech Publishing, 2005.